Norges miljø- og
biovitenskapelige
universitet

Master's Thesis 2016 60 ECTS
Norwegian University of Life Sciences
Department of Chemistry, Biotechnology and Food Science

An in vitro model for determining the chemo-sensitizing effects of hyperthermia on ovarian cancer cell lines

Theodor Malmer Herud
Chemistry and Biotechnology, Molecular Biology

Acknowledgements

This master thesis was completed during the period of August, 2016, to May, 2017 at the Institute for Cancer Research, Radium Hospital, at the Department of Tumor Biology led by Gunhild Mari Mælandsmo.

First and foremost, I would like to thank my brilliant supervisor Dr. Yvonne Andersson; this master thesis is molded by all our frequent discussions and stimulating conversations. I am grateful for your continuous support and guidance, for believing in me and allowing me the freedom to explore scientific ideas out of shared curiosity.

Thank you, Dr. Kjersti Flatmark, for welcoming me into your multidisciplinary research group. To all members of the research group, thank you for enjoyable discussions, for sharing inspiring scientific explorations and for all support.
I am grateful to prof. Gunhild Mari Mælandsmo for allowing me to write my thesis at the Department of Tumor Biology. To all researchers at the Department: thank you for any and all help, scientific training, enjoyable conversations and, every so often, for delicious cake.

I would also like to thank Karine Flem Karlsen, for enthusiastically teaching a newcomer several essential laboratory techniques; Siri Tveito, for kindly sharing her Peggy Sue expertise; and Idun Dale Rein, for assistance and lessons in Flow Cytometry. I thank prof. Ragnhild Lothe, head of the Department of Molecular Oncology, for opening the doors to the Institute for Cancer Research and setting the wheels in motion. To Sarina, Kjetil, Wafa, Christell and all my fellow master students at the Department; it has been a pleasure to study beside you.

Finally, I owe thanks to my family for always providing overwhelming encouragement, support and enthusiasm in challenging times.

Theodor M. Herud

Sammendrag

I Norge dør omlag 300 kvinner hvert år av eggstokk-kreft. Sykdommen er vanskelig å oppdage og vil i de fleste tilfeller være på avansert stadium ved første diagnose. Avansert eggstokk-kreft danner ofte metastaser i bukhulen, og ordinær behandling består av avansert kirurgi og systemisk kjemoterapi. Dessverre er slik behandling lite effektiv og en stor andel pasienter vil få tilbakefall som følge av gjenværende kreftceller, noe som fører til en svært lav 5-års overlevelsesrate.

Hypertermisk intraperitoneal kjemoterapi (HIPEC) er en unik metode satt sammen for å behandle mikroskopiske tumorer og frie kreftceller i bukhulen etter kirurgi. Metoden benytter oppvarmet cellegift som sirkuleres direkte i bukhulen, og kliniske forsøk på pasienter med peritoneal spredning av eggstokk-kreft har vist økt overlevelsesrate. Likevel er det svært få pre-kliniske studier som undersøker hvordan kombinasjonsbehandling med hypertermi påvirker kreftceller på et molekylært nivå, og manglende kunnskap gjør det vanskelig å forbedre det kliniske utfallet til HIPEC.

I denne masteroppgaven etablerte vi en in vitro modell som etterlikner forholdene under en HIPEC-prosedyre. Målet var å undersøke om kombinasjonsbehandling med hypertermi og cellegift eller immunotoksin kunne påvirke levedyktighet, celledød og cellesyklus i ovariekreft-cellelinjer. MTS viabilitets-assay ble benyttet for å undersøke levedyktighet etter behandling, mens TUNEL apoptose-assay og Hoechst-DNA farging ble brukt til å undersøke celledød og cellesyklus-distribusjon gjennom flow cytometri. I tillegg ble ekspresjonsnivået av HSP70 undersøkt i cellelinjene ved bruk av PeggySue™ teknologi, ettersom proteinet tidligere har blitt knyttet til terapi-resistens.

Forsøksresultatene viste at hypertermi kan øke effekten av cellegift, men at denne effekten varierer avhengig av cellelinje. Cellelinjen OVCA432 hadde høy resistens basert på viabilitetsmålinger, og hadde høyest økning i HSP70 ekspresjon etter hypertermi. Av de tre cellegiftene var det cisplatin som oftest viste synergi i kombinasjon med hypertermi, mens immunotoksinet MOC31PE var det eneste

middelet som viste synergi med hypertermi i alle cellelinjene. Den carboplatin-resistente cellelinjen B76 ble sensitiv mot carboplatin i kombinasjon med hypertermi. For å verifisere in vitro resultater kan ex-vivo pasientmateriale og dyremodeller inkorporeres i fremtidige forsøk, samt ulike teknikker for å undersøke celledød etter behandling. Videre forsking på kartlegging av gener som underbygger den observerte resistensen til OVCA433 eller OVCA432 kan bidra til å utvikle strategier som reverser terapi-resistens, samt forbedre selektsjon av cellegifter som drar nytte av hypertermi.

Abstract

Ovarian cancers, the deadliest of gynecological malignancies, claim the lives of 300 Norwegian women every year. The disease is characterized by late stage detection and the majority of patients present peritoneal metastases upon first diagnosis. Conventional treatment consists of cytoreductive surgery and intravenous chemotherapy, but treatment is ineffective at removing all residual disease and the majority of patients relapse, resulting in 5-year survival rates less than 34%.

Hyperthermic intraperitoneal chemotherapy (HIPEC) is a method constructed to remove microscopic metastases and free cancer cells within the peritoneal cavity after cytoreductive surgery. The procedure involves circulating heated chemotherapy directly into the peritoneal cavity, and clinical trials on metastatic ovarian cancer have shown survival benefit. However, few studies have investigated the effect hyperthermia has on cancer cells during HIPEC, and limited knowledge prevents improvements to the HIPEC procedure and drug selection.

During this master thesis we established an in vitro model replicating the clinical conditions of HIPEC. The aim was to investigate the effects of hyperthermia treatment combined with chemotherapy or immunotoxin on the viability, apoptosis and cell cycle distribution of ovarian cancer cell lines. Viability was assessed with MTS-assay, while TUNEL-assay and Hoechst DNA-stain was used to analyze apoptosis and cell cycle distribution by flow cytometry. Expression levels of HSP70 were investigated using PeggySue™ technology, as HSP70 expression has been linked to therapy resistance.

The results show that hyperthermia can sensitize cells to chemotherapy, but the extent of this effect varies among the cell lines. The cell line OVCA432 had highest resistance based on viability measurements, while also having the highest increase in HSP70 expression after hyperthermia. Of the three chemotherapy agents included in this study, the effect of cisplatin was most frequently potentiated by hyperthermia. We also found the carboplatin-resistant cell line B76 to be sensitized

by hyperthermia during analysis of apoptosis. The immunotoxin MOC31PE was the only agent showing hyperthermia sensitization in all cell lines. Limitations of the model include the use of viability assays to determine cell response, as well as cell cultures. These limitations can be resolved by incorporating ex-vivo patient samples or animal models, and by including several methods of analyzing treatment response. Our findings show that the sensitizing effect of hyperthermia may depend on the patient-specific tumor profile. Future studies should aim to investigate candidate genes for the resistance observed in cell lines OVCA433 and OVCA432, which could facilitate development of strategies that reverse treatment resistance, and improve the selection of drugs which benefit from HIPEC administration.

Abbreviations

ADP	Adenosine diphosphate
ATP	Adenosine triphosphate
B-actin	Beta-actin
BCA	Bicinchoninic acid
BRCA1/2	Breast cancer susceptibility gene 1 and 2
BSA	Bovine serum albumin
CC	Completeness of cytoreduction
COSMIC	Catalogue of Somatic Mutations in Cancer
CRS	Cytoreductive surgery
DMSO	Dimethyl sulfoxide
DTT	Dithiothreitol
EDTA	Ethylenediaminetetraacetic acid
EMT	Epithelial-to-mesenchymal transition
EOC	Epithelial ovarian cancer
EpCAM	Epithelial cell adhesion molecule
GAPDH	Glyceraldehyde 3-phosphate dehydrogenase
HSA	Human serum albumin
HIPEC	Hyperthermic Intraperitoneal Chemotherapy
HSP	Heat shock protein
HT	Hyperthermia
I.P.	Intraperitoneal
I.V.	Intravenous
IC50	Half maximal inhibitory concentration
kDa	Kilo-Daltons (atomic mass unit)
LDS	Lithium dodecyl sulfate
NHEJ	Non-homologous end-joining
OC	Ovarian cancer
PBS	Phosphate buffered saline
PCI	Peritoneal carcinomatosis index
PE	Pseudomonas exotoxin
PFI	Platinum-free interval
PM	Peritoneal metastases
PVDF	Polyvinylidene difluoride (membrane)
RMPI-1640	Roswell Park Memorial Institute medium 1640
SDS	Sodium dodecyl sulfate
TBS-T	Tris-buffered saline with Tween 20
TUNEL	Terminal deoxynucleotidyl transferase (TdT) dUTP Nick-End Labeling
UPR	Unfolded-protein response
µM	Micromolar (micromoles/liter)
ng/ml	Nanogram per milliliter

Table of contents

1 Introduction

1.1 Cancer

Cancer encompasses a large group of diseases characterized by abnormal growth and spread of cancerous cells from the site of origin. Traditionally viewed as a disease of the genome, cancer is thought to arise in normal cells by an accumulation of genetic mutations and epigenetic modifications which disrupt the normal function of signaling pathways responsible for coordinating cell death, differentiation and proliferation. Cancer research has provided important insights to the molecular basis of cancer development, but no universal cure has been discovered. The plasticity of cancer remains the largest hurdle in our pursuit of therapies against a disease which claim nearly 8 million lives every year [1].

1.1.1 Cancer development

The development of cancer begins with mutations. Mutations are modifications of the DNA sequence capable of altering gene expression, for instance by changing nucleotide sequences within promoter or coding regions of a gene. Mutations are introduced to DNA by exposure to environmental carcinogens, both exogenous and endogenous, but also through the inherent error-prone DNA replication and repair machinery. Approximately 3 mutations are formed from unrepaired errors induced by DNA polymerases during each stem cell replication, and the total number of stem cell divisions have been shown to correlate with cancer formation [2]. As stem cells continue to replicate throughout our lives, it is not surprising that risk of developing cancer increases with age [3].

Inherited gene alterations can increase the likelihood of acquiring mutations required for transforming a normal cell into a cancerous cell [4]. For instance, the breast cancer susceptibility genes 1 and 2 (BRCA1 and BRCA 2) are tumor-suppressor genes crucial for initiating repair of DNA double-strand breaks by homologous recombination (HR). Women with inherited germ-line mutations in

BRCA1/2 have higher risk of developing breast and ovarian cancer mainly because loss of HR favors the less-accurate non-homologous end-joining (NHEJ) repair pathway, which increases mutation rates and causes genomic instability [5, 6].

When mutations occur in genes which serve as working end-points of cell signaling cascades, the effect can be tumorigenic (tumor-enabling). Such genes are often referred to as tumor-suppressor genes, and include regulators of DNA integrity and cell cycle checkpoints, as well as cell death pathways (apoptosis). Loss of tumor-suppressor genes can promote tumor formation, and is evident in the high frequency of cancers with mutations in the tumor-suppressor p53 [7]. Proto-oncogenes, on the other hand, regulate and promote cell proliferation and survival. Mutations in proto-oncogenes can turn them into oncogenes, in which case their growth-promoting activity is increased. In theory, transformation from normal to uncontrolled growth state can be viewed as a cumulative effect of activated oncogenes and inactivated tumor-suppressor genes.

1.1.2 Tumor formation and metastasis

Cells that grow uncontrolled are called neoplasms, and neoplasms often form solid aggregations called tumors. Not all tumors are cancerous; benign tumors are unable to cross tissue borders and invade adjacent tissues. Tumors are abnormal structures mainly consisting of growing neoplasms, supporting stromal cells, immune cells and recruited neovessels. While initially unable to invade other tissues, benign tumors often become malignant over time. The gradual progression from a benign to a malignant state is a process involving distinct differentiation pathways and interactions between cancer cells and the tumor microenvironment [8]. Indeed, an important step in malignant transformation of epithelial cancer cells, called the epithelial-to-mesenchymal transition (EMT), is largely controlled by signals from the normal cells within the tumor [9-11]. It has been suggested that tumor formation is a direct consequence of disrupted tissue integrity, where degenerative mutations within normal cells of the tissue might precede tumor formation [12, 13].

Cancer cells that become malignant can migrate away from the primary tumor, re-attach and form secondary tumors called metastases. Wherever a new tumor forms, selection of mutations that confer a growth advantage will occur within the cancer population [14]. As a result, patients can have highly heterogeneous populations of cancer cells, both within each tumor and between separate metastases. Meanwhile, a fraction of cancer cells may acquire mutations or epigenetic modifications which confer resistance to cancer treatments, either spontaneously, through microenvironment signaling, or as direct result of selection pressure caused by drug exposure. This explains why many cancers first appear treatment responsive but eventually relapse; it is the death of susceptible cancer cells, followed by the inevitable regrowth of the resistant, and often dormant, cancer subpopulation [15].

The mechanisms responsible for drug resistance in cancer are not fully understood, but include both intrinsic and microenvironment processes [16, 17]. A portion of resistance mutations have been shown to be shared by many cancers and are, ironically, promising drug targets [18]. The inherent plasticity of cancer means two things for cancer therapy; first, each cancer is unique and contains both tissue-specific and patient-specific genetic variation, which should be determined prior to drug selection to maximize treatment efficacy. Secondly, and analogous to strategies used to avoid multi-drug resistance in bacteria, combining and cycling drugs which target different molecular pathways is a potential strategy for deterring resistance development.

1.2 Ovarian cancer

According to the Norwegian Cancer Registry, around 300 Norwegian women die annually from ovarian cancer (OC) [19]. Nicknamed “the silent killer”, patients diagnosed with the disease are faced with the overall worst prognosis and lowest survival rate out of all gynecological malignancies. Less than one-half of all patients will survive more than 5 years after diagnosis. Despite being a major cause of cancer related deaths in women, research efforts on OC therapy have failed to markedly improve the overall survival rate [20]. Early stage OC can be cured by surgery as

over 90% of patients with localized disease will survive past the 5 year mark. Sadly, only 1 in 5 ovarian cancers are detected at the early stage.

Late stage detection is characteristic of OC. Classified as retroperitoneal, the ovaries are embedded into the broad ligament on both sides of the uterus and partly suspended into the peritoneal cavity. The many layers of tissue, fat and organs surrounding the ovaries complicate screening and prevent early tumor detection. In addition, early symptoms of ovarian cancer are often non-specific and mild, concealing the disease and delaying diagnosis until more severe symptoms develop [21].

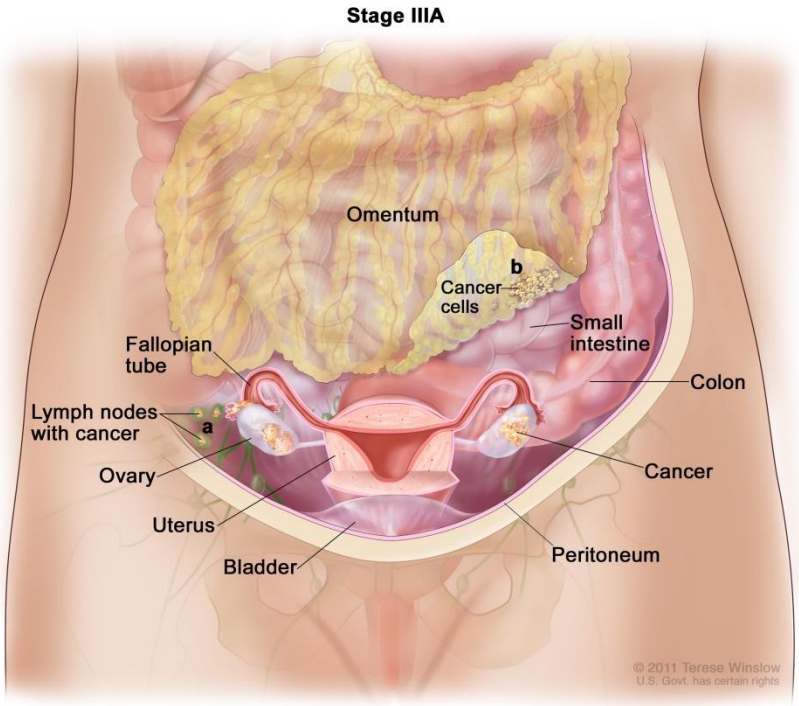

Figure 1: Stage IIIA ovarian cancer has spread to nearby lymph nodes in the pelvis and to the peritoneum. Terese Winslow, 2011, National Cancer Institute. Adapted from: https://www.cancer.gov/types/ovarian/patient/ovarian-epithelial-treatment-pdq#section/_130

As the cancer progresses, it can spread to nearby organs of the pelvis including the uterus, the colon and the bladder (figure 1). Metastatic OC are known to invade nearby lymph nodes, organs within the peritoneal cavity, as well as distant tissues beyond the abdominal area through the circulatory and lymphatic systems. In

addition, 30% of ovarian cancer patients have malignant ascites – single and aggregated cancer cells suspended in peritoneal fluid in the abdomen – which are thought to form when cancer cells detach from primary tumor and "seed" directly into the peritoneal cavity. Malignant ascites is associated with treatment resistance and poor prognosis [22].

1.2.1 Classification of ovarian cancer

OC constitute a heterogeneous group of neoplasms thought to arise from cells located within or on the surface of the ovaries. Several classification systems of OC have been proposed based on cell-type of origin, histology and degree of differentiation, or association with disease stage and pathology. In general, OC develop in either epithelial, germ-line or sex cord-stromal cells. Epithelial ovarian cancers (EOC), commonly referred to as ovarian carcinomas, are by far the most prominent and comprise nearly 90% of all OC [23]. EOC have been classified by the World Health Organization (WHO) into low- and high-grade serous, mucinous, endometrioid and clear cell carcinomas, in addition to transitional and undifferentiated tumors [24].

Another classification system divides OC into type 1 or type 2 disease [25]. Type 1 includes the subtype low-grade serous, mucinous and low-grade endometrioid carcinoma, which proliferate slowly and are thought to be confined locally for longer periods. In contrast, Type 2 constitutes high-grade serous and high-grade endometrioid carcinoma, subtypes with more aggressive phenotypes linked to poor prognosis. The most frequent genetic alterations of type 1 disease include mutated BRAF and KRAS genes of the mitogenic pathway, while type 2 OC typically have mutations in the tumor-suppressor TP53 [26]. Determining cancer subtype by biopsy can be useful prior to selection of therapeutic strategy, as the genetic profiles of each subtype have been linked to treatment response and prognosis [23, 27]. The dominating subtype of OC is high-grade serous ovarian carcinoma (HGSOC). It constitutes near 80 % of all OC and is responsible for the vast majority of mortalities

[28]. Improving the treatment of HGSOC is therefore crucial for reducing OC mortalities.

1.2.2 Peritoneal metastases in ovarian cancer

While patterns of metastatic spread vary among patients and cancer subtype, the most prominent site of colonization is the peritoneal cavity. Over two-thirds of patients with advanced stage OC present peritoneal metastases (PM) at disease discovery, and it is the main site of recurrence after primary treatment [29]. Peritoneal metastases present a unique challenge for surgeons, as cancer cells can disseminate onto abdominal organs and the large volume of mesenteric tissue which connects them. Type 2 OC, thereby mainly HGSOC, have been found to metastasize to the peritoneal cavity much more frequently than type 1 disease [30].

1.3 Treatment of ovarian cancer

Conventional treatment of OC consists of cytoreductive surgery (CRS) followed by intravenous chemotherapy, commonly a platinum (cisplatin or carboplatin) and taxane combination. Platinum-based drugs kill rapidly proliferating cells by forming crosslinks in DNA, while taxanes stabilize microtubules. The initial response to chemotherapy is often high, but almost always followed by relapse of therapy-resistant disease. The time it takes for the disease to relapse after platinum chemotherapy, known as the 'platinum-free interval' (PFI), is used to classify OC into platinum sensitive (>12 months), partially sensitive (6-12 months), resistant (<6 months), or platinum refractory if treatment fails to induce disease remission. In general, shorter PFI is linked with poor prognosis [31].

The poor prognosis of therapy-resistant recurrent OC is due to the lack of effective therapy alternatives. Increasing dose-intervals is mostly counterproductive as chemotherapy agents become less effective each cycle due to resistance development, while still causing severe side-effects due to their non-discriminatory mode of action [32]. To avoid unnecessary morbidity caused by ineffective platinum therapy, researchers have attempted to map molecular markers of platinum resistance [33,

34]. While studies have reported high accuracy in predicting treatment response based on markers during ex vivo analysis [35], it is currently unclear if marker-assisted treatment can be implemented clinically without the risk of false negatives.

1.3.1 Intraperitoneal chemotherapy

Intraperitoneal (IP) chemotherapy refers to administration of chemotherapy directly into the peritoneal cavity. The main benefit comes from low systemic uptake of drugs through the blood-peritoneal barrier, especially drugs of high molecular weight and low water solubility, such as taxanes [36, 37]. The phenomenon allows high drug concentrations to be in direct contact with microscopic tumors or detached cancer cells (including ascites), while maintaining acceptable systemic toxicity. Targeting and effectively removing metastases and free cancer cells in the peritoneal cavity is crucial for disease outcome. The main issue with IP chemotherapy is that drug penetration is limited by tumor size, and treatment efficacy often depends on the outcome of CRS. Combining IP and intravenous (IV) chemotherapy has, however, shown survival benefit [38, 39].

1.4 Hyperthermic intraperitoneal chemotherapy (HIPEC)

Hyperthermic Intraperitoneal Chemotherapy (HIPEC) combines IP chemotherapy with hyperthermia (HT). It was first introduced as a method to treat peritoneal metastases in patients with colorectal cancer, but is now becoming a prominent alternative for the management of peritoneal metastases in general. Use of adjuvant HT in the high-fever range (41-43ºC) is thought to increase drug penetration into microscopic disease, a factor known to limit the efficacy of IP chemotherapy.

1.4.1 The HIPEC procedure

HIPEC is administered shortly after CRS by an open or closed technique. In the open technique, the abdominal wall is lifted around the site of incision, creating an open 'reservoir' (figure 2). Open HIPEC has the advantage of additional control, as surgeons can monitor the procedure and ensure proper circulation of the drug perfusate. In the closed technique, tubes inserted into abdominal incisions direct the

flow of the heated chemotherapy solution. Closed HIPEC can also be combined with laparoscopy[40]. Regardless of technique, chemotherapy circulation rarely exceeds 2 hours.

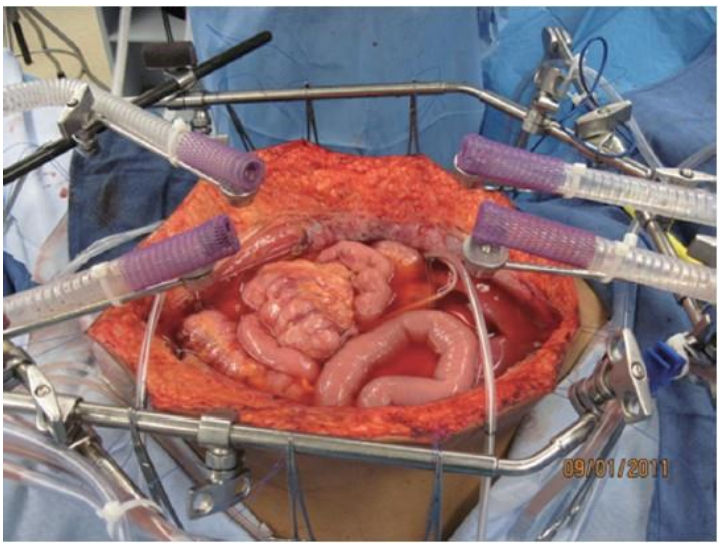

Figure 2: Hipec administered using the 'open' technique. Sugarbaker PH, Stuart OA, Bijelic L. 2012 [41]. Retrieved from: http://tgc.amegroups.com/article/view/949/1131

Prior to HIPEC administration is CRS, i.e. surgical removal of metastases and resecting of disease-ridden tissue. The success of CRS is commonly reported as 'completeness of cytoreduction' (CC) and scored from 0 to 3, where 0 = no visible disease and 3 = single or merged tumor nodules >2.5cm [42]. HIPEC is rarely considered if complete CRS is impossible, as it diminishes treatment efficacy and survival benefit. Both the total extent of peritoneal spread, measured by the 'Peritoneal Cancer Index' (PCI), and CC-value have been shown to be strong prognostic factors for HIPEC outcome [42, 43].

Although HIPEC has been adopted by a handful of hospitals around the world, treatment guidelines vary among countries. As a result, clinical results from HIPEC trials can be difficult to compare due to variations in treatment duration, selection of drug(s) and their concentration in the perfusate, methods of patient selection, temperatures achieved in the peritoneal cavity, surgical procedure (CRS) and instruments used. HIPEC is undoubtedly an intensive medical procedure, and treatment outcome depend on the experience and skill of the surgical team. The

morbidity previously associated with HIPEC can be expected to decrease as hospitals gain experience, both procedurally and in selecting patients which will benefit from the treatment. However, drug selection is still crucial for treatment outcome. Recent clinical data show favorable survival benefit from HIPEC for recurrent OC [44], resulting from improved control and removal of peritoneal disease. Lack of pre-clinical studies on the drug-HT interaction is, however, likely limiting the full potential of HIPEC for OC.

1.5 Sensitization by hyperthermia

Local HT (41-43ºC) achieved during HIPEC induces several physiological changes (figure 3), including vasculature opening and increased blood flow which can lead to oxygenation of hypoxic tumor regions and increase in reactive oxygen species (ROS) formation [45].

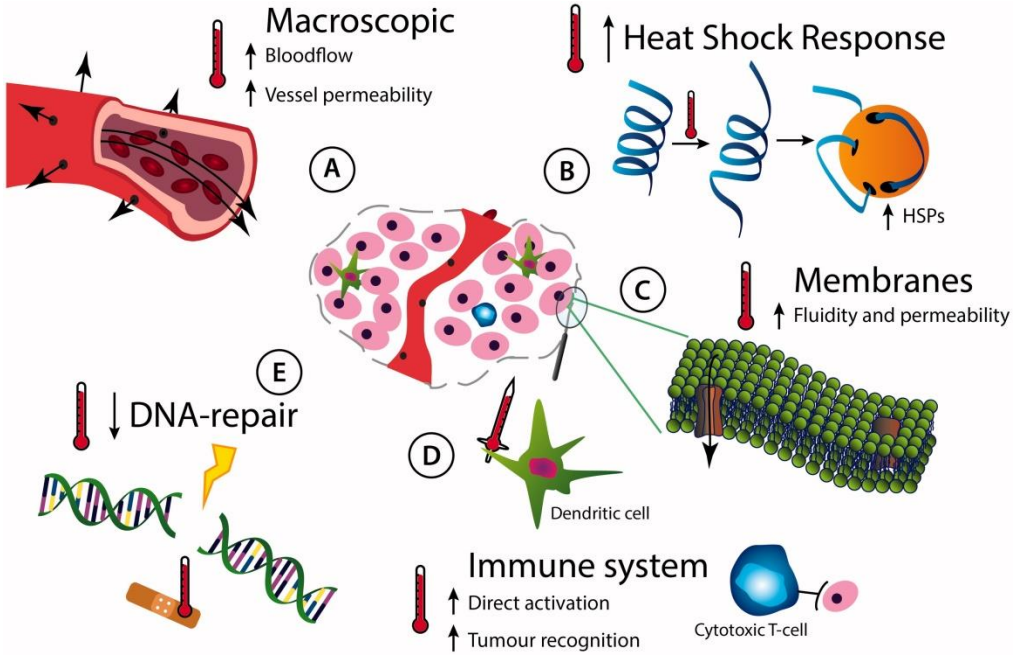

Figure 3: The various effects of HT on tissue and within cells can be advantageous for cancer therapy [46]. Adapted from: http://www.tandfonline.com/doi/full/10.3109/02656736.2016.1157216

HT increases the motility of dendritic cells and T-cells, and can be a modulator for the anti-cancer activity of the immune system [47-49]. While physiological and immunological changes occur during HT, it is unclear to what extent they impact

HIPEC treatment efficacy. The main rationale for use of adjuvant HT during HIPEC is its cytotoxic effect on cancerous cells. The mechanisms of HT-induced cancer cell death are poorly understood, but are thought to include inhibition of the DNA repair machinery [50-52], loss of mitochondria membrane potential [53], ROS generation [54], as well as an accumulation of misfolded and aggregated proteins [55].

Many of the suggested molecular effects of HT can synergize with cancer therapy, by increasing the potency of chemotherapy agents or reducing cellular resistance – a phenomenon known as chemo-sensitization. However, there is a lack of pre-clinical data investigating the molecular mechanisms responsible, and as a result, clinical adaption is lagging behind. HIPEC is a treatment that could benefit by selecting drugs which synergizes with HT administration.

1.5.1 Heat shock proteins

HT also lead to protein misfolding, and cells have sophisticated stress-response systems which monitor and protect the cell from damage caused by HT, oxidative stress and other factors which destabilize proteome homeostasis. The two main regulatory systems of proteome stability are the unfolded protein response (UPR) and the heat-shock response (HSR) [56]. Both the UPR and the HSR systems have been shown to be modulated in many cancers, likely a result of a constitutively stressed state caused by altered metabolism, abnormal proliferation and characteristics of the tumor environment, including hypoxia, inflammation and ischemia. Both stress response systems induce heat shock protein (HSP) expression.

The heat shock proteins comprise a large family of molecular chaperones which maintain protein stability and protect the cell during stress conditions. Although their primary function is to maintain proteasome homeostasis by chaperone activity, HSPs also partake in cell signaling pathways, transport of client proteins and regulation of oxidative stress [56]. Several HSPs, including heat shock protein 70 (HSP70) and heat shock 27 (HSP27), have anti-apoptotic functions as well as immunogenic properties [57, 58]. In addition, the expression of HSPs has been

shown to increase during chemotherapy and is linked to treatment resistance in cancer [59-61]. The expression of heat shock proteins is abnormally high in many cancers, and their cytoprotective functions can promote tumorigenesis [62]. Because of their anti-apoptotic functions and their involvement in treatment resistance, HSP are becoming promising targets in cancer therapy [56]. Several HSP inhibitors are have undergone clinical trials, including the HSP70 inhibitor Pifithrin-μ [63] the HSP90 inhibitor 17-AAG [64].

2 Aims of the study

HIPEC is becoming a prominent alternative for treatment of metastatic ovarian cancer. Several aspects regarding HIPEC remain unknown, however, including the effect of HT on cancerous cells and its interactions with chemotherapeutics. While clinical trials with HIPEC are ongoing, the lack of pre-clinical research on drug combinations which synergize with HIPEC administration is limiting its potential; it is also impeding further adaption and improvement of the HIPEC procedure.

In this study, we wanted to establish an in vitro model replicating the conditions of HIPEC treatment in patients, and use the model to investigate the response of cell lines to treatment with HT and chemotherapy. We wanted to examine the role of HSP70 expression in treatment response, and in addition to conventional chemotherapy agents included the novel immunotoxin MOC31PE as a potential candidate for HIPEC.

This study can be separated into four main aims:

- To establish an in vitro model mimicking HIPEC conditions and observe the effect of combination treatments on viability of a HGSOC cell line panel
- To examine rate of apoptosis and cell cycle distribution after cell line treatment by flow cytometry, to explain the effects of combination treatment at a cellular level
- To investigate the role of HSP70 expression for cell line response to treatment
- To measure the effect of MOC31PE treatment on cell line viability and determine its potential for HIPEC treatment

3 Methods

3.1 Cell culturing

Five OC cell lines were used in this study. Cell lines B76, OVCA433 and OVCA432 were kindly provided by Dr C. Marth at Innsbruck Medical University (Innsbruck, Austria) [65, 66], CaOV3 was purchased from American Type Culture Collection (ATCC, Manassas, Virginia), and the patient derived peritoneal metastasis (pm) OC cell line pmOC8 was recently established in our laboratory by Dr. Andersson (Department of Tumor Biology, Radium Hospital, Norway).

All cell lines were grown in RPMI-1640 medium supplemented with 10% fetal bovine serum (FBS), 2% HEPES buffer solution, 1% alanyl-glutamine (ala-gln), 100 units/ml penicillin and 100 µg/ml streptavidin. RPMI-1640 contains amino acids, mineral salts, vitamins and glucose required for cell growth, while FBS contains high levels of growth factors which stimulate cell proliferation. HEPES buffer was added to maintain stable pH, while alanyl-glutamine, a stabilized form of the amino acid L-glutamine, was added as it is required for both protein synthesis and metabolism within cells. For the remainder of this thesis, the complete RPMI medium described above will be referred to only as medium. All cell culture consumables mentioned were purchased from Sigma-Aldrich©.

Cell lines were cultured in nuncleon™ EasYFlask™ T25, T75 or T150 (Thermo Scientific), and incubated at 37ºC in a humidified atmosphere with 5% CO_2 (Heracell™ 150i). Cell cultures were maintained at 2-dimensional growth and passaged at 80-90% confluence by addition of 0.25% trypsin-EDTA (ethylenediaminetetraacetic acid; Sigma). Trypsin is a proteolytic enzyme which cleaves cellular adhesion molecules (CAM), while EDTA chelates ions that may disrupt trypsin function. As trypsin can damage cell membranes, it was always disabled with medium immediately after cell detachment.

For long term storage, cells were dissolved in RPMI-1640 medium containing 20% FBS and 10% dimethyl sulfoxide (DMSO; Sigma) and frozen at -80ºC. When a cell

line reached over 20 passages, it was discarded and a frozen sample was thawed. Cell culture work was done in a sterile environment, and all cell lines were tested for mycoplasma. The cell lines CaOV3, OVCA432 and OVCA433 were initially cultured in Dulbecco's Modified Eagle's Medium (DMEM; Sigma). For convenience, DMEM medium was substituted with RPMI-1640 medium for all cell lines as it yielded similar growth rates.

3.2 Chemotherapy drugs

The chemotherapy drugs used in this study were cisplatin, carboplatin and mitomycin-C (mitomycin). Cisplatin was purchased from Accord Healthcare, mitomycin from MedacPharma Inc. and carboplatin from Hospira Nordic AB. Mitomycin solutions were prepared by dissolving mitomycin stock powder (2 mg, Medac) in phosphate buffered saline (PBS;Sigma). Cisplatin (1 mg/ml) and carboplatin (10 mg/ml) came in stock solutions of containing 0.9% saline. For single-drug screening, serial dilutions of the drugs were made in RPMI-1640 medium. The three chemotherapy drugs were selected based on relevance and prior use in HIPEC. Cisplatin (cis-diamminedichloridoplatinum(II)) and carboplatin (Cis-Diammine(1,1-cyclobutanedicarboxylato)platinum(II)) are both platinum-based compounds that form crosslinks in DNA. The main mechanism of mitomycin (methylazirinopyrroloindoledione) is DNA alkylation, although other pathways have been suggested [67]. All laboratory work involving chemotherapeutics was done in class 2 safety cabinets after special training.

The immunotoxin MOC31PE (0.5 mg/ml in PBS with 0.1% human serum albumin (HSA)) was also included in the study [68, 69]. MOC31PE has been developed at the Department of Tumor Biology (Institute for Cancer Research, Radium Hospital, Norway), and has recently completed clinical trials [70, 71]. MOC31PE is composed of a MOC-31 monoclonal antibody targeting epithelial cell adhesion molecule (EpCAM), conjugated to a Pseudomonas exotoxin A (PE) [72-74]. Serial dilutions of MOC31PE immunotoxin were made with 0.1% human serum albumin in PBS.

3.2.1 Selecting drug concentrations

In vitro drug concentrations were selected based on the clinical HIPEC drug concentrations reported in literature (table 1). Calculation of representative dose was made by using an average human body mass of 1.7 ($m^2 = 1.7$). A concentration range was included in experiments to allow investigation of drug effect at half or double clinical concentration.

Table 1: Drug concentrations from clinical HIPEC and the selected in vitro concentrations

Drug	HIPEC concentration range [44, 75, 76]	Calculated concentration for in vitro treatment
Mitomycin-c	15-30 mg/m2/L	60 μM
Cisplatin	25-70 mg/m2/L	75 μM
Carboplatin	175-600 mg/m2/L	250 μM

3.3 Hyperthermic drug treatment

To investigate the effect of HT on cancer cells during HIPEC, the experimental in vitro model had to replicate the conditions achieved in patients during HIPEC treatment as close as possible. The cell line treatment needed to: (1) represent ovarian cancer (preferably HGSOC), (2) replicate drug concentrations obtained clinically, and (3) allow limited duration of cell exposure to drug and HT. The selected HT temperature for the study was 42ºC, as it is the average reported temperature [44].

Protocol

Cells were harvested at 75-85% confluence from culture flasks by addition of 0.25% trypsin-EDTA, followed by medium and centrifugation at 1000g for 5 minutes before cells were suspended in new medium. Cell concentration was determined manually using a Bürker cell counting-chamber (Hecht-Assistent®) under a light microscope (Olympus CKX41). Solutions of mitomycin, cisplatin, carboplatin or MOC31PE were prepared in 15 mL plastic centrifuge tubes by mixing drug with medium to 1 ml solutions. After cells were counted, 1 ml of cell suspension was distributed to each tube containing prepared medium-drug mixture or medium only (control). After gentle mixing, cell-drug-suspension was split equally to two 15 ml centrifuge tubes

which were placed in separate temperature controlled water baths set to 37ºC and 42ºC (figure 4). Both water baths were high precision temperature controlled, and temperature was verified throughout the experiments with glass thermometers (Cole-Parmer®). Water baths were found to keep stable temperature, but occasionally deviated ± 0.3 ºC, mainly during sample insertion.

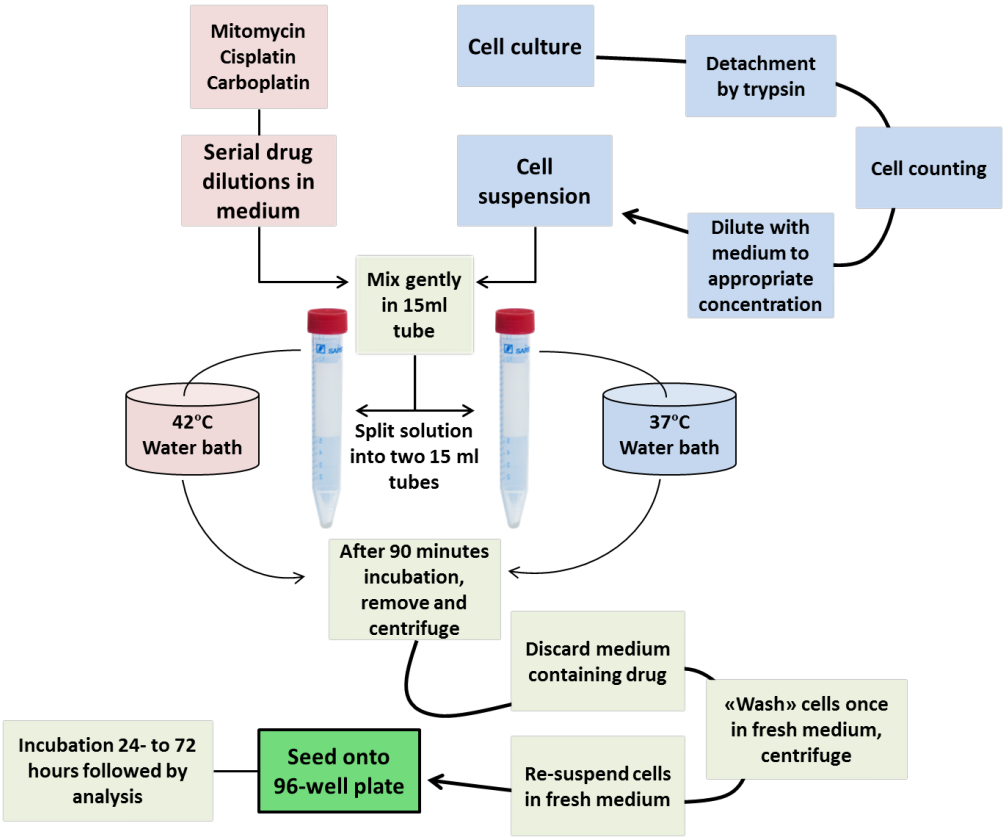

Figure 4: Overview of the different steps in the treatment protocol. For MOC31PE, serial dilutions were made in PBS with 0.1% HSA, but otherwise the protocol was identical.

Tubes were removed from the water baths after 90 minutes and centrifuged at 1000 g for 5 minutes (Heraeus Megafuge 1.0). Medium was discarded, and cells were washed once with medium to remove residual drug, centrifuged (1000g x 5 min) and suspended in new medium. Cells were finally seeded in triplicate (100 µl/well) onto nuncleon™ 96-well plates for MTS assay, nuncleon™ 96-well white-walled plates for ATP assay, or nuncleon T25 (25 cm^2) flasks for flow cytometry or protein analysis. Cells were incubated at 37ºC with 5% CO_2 for a maximum of 72 hours before experiments were continued. For MTS assays, cells were seeded equally onto two 96-

well plates to allow viability measurements after 24 and 72 hours, respectively. Data obtained from viability assays after 24 hours were used to determine the relative increase in proliferation within individual samples.

3.4 Measuring the effect of treatment on cell viability

Cell viability assays are used to assess the relative health status of cells. They are extensively used in cancer research as they allow fast, high-throughput analysis of cell response to drug treatment. It should be noted that cell viability assays measure only the relative or 'total' viability based on a vehicle control, and cannot be used to distinguish between strictly cytostatic or cytotoxic drug effects without further assessment. In this study, cell viability assays were used to determine the effect of drug and HT treatment on cell proliferation based on a vehicle control (medium only). Other methods of analysis, including TUNEL-assay, were applied later to support viability data.

3.4.1 MTS Assay

Cell viability was assessed using the MTS-based CellTiter 96® AQueous One Solution Cell Proliferation Assay (Promega). The assay is based on a tetrazolium dye [3-(4,5-dimethylthiazol-2-yl)-5-(3-carboxymethoxyphenyl)-2-(4-sulfophenyl)-2H-tetrazolium], which can be reduced to a stable and colored formazan-complex. Reduction of the tetrazolium dye is dependent on reductase enzymes present within living cells. The total number of viable cells present in a sample will determine color intensity, which can be measured using a spectrophotometer.

Protocol

Cell viability was analyzed by MTS assay 24- and 72 hours after combination treatment (see section 3.3.1). The MTS-reagent was added in a 1:10 volume ratio to each well and incubated for 2 hours at 37ºC, and absorbance was measured at 450 nm with a Modulus™ Microplate-reader (Turner Biosystems). To prevent cell confluence during plate incubation, cell-line specific proliferation rates were experimentally determined and taken into account prior to seeding. The cell lines

B76, CaOV3 and pmOC8 were seeded at 15'000 cells/well, while cell lines OVCA432 and OVCA433 were seeded at 10'000 cells/well.

3.4.2 ATP assay

The CellTiter-Glo® Luminescent Cell Viability Assay (Promega) was used to supplement viability data obtained from the MTS-assay. The CellTiter-Glo® assay is based on recombinant thermostable luciferase, an enzyme capable of bioluminescence in presence of its substrate adenosine triphosphate (ATP). As luminescence intensity correlates with the amount of ATP molecules present, it can be used to estimate the relative amount of metabolically active and thereby viable cells. The ATP assay was only used initially during the first experiment on a new cell line to ensure that the MTS assay provided reliable data.

Protocol

The two CellTiter-Glo® reagents were mixed according to producer manual, added to each well in a 1:1 reagent-to-medium volume ratio and incubated for 10 minutes on a plate mixer. Luminescence signal was measured on a Modulus™ Microplate-reader (Turner Biosystems). White-walled 96-well plates were used to ensure minimal signal noise from adjacent wells during analysis.

3.5 Protein analysis

The expression of heat shock proteins is known to be affected by cellular stress and have been shown to be associated with treatment resistance in cancer [56, 77]. To determine the expression of heat shock proteins in the cell lines before and after treatment, two immunoassay-based methods were applied: western blot and Peggy Sue™. Both methods measure the amount of protein based on the binding of antibodies to protein of interest. Before the methods can be used, however, cells must be lysed, a process where cellular membranes are disrupted to release their intracellular content.

Cells were lysed on ice with buffered solutions containing NP-40 (Abcam), a detergent which disrupts membrane integrity, PhosSTOP™ (Sigma) and

cOmplete™ (Sigma). PhosSTOP™ and cOmplete™ contain phosphatase and protease inhibitors, respectively, which prevent protein degradation. For a complete list of reagents in the lysis buffer, see appendix 1. Protein lysates were analyzed using the bicinchoninic acid (BCA) - assay (Thermo Scientific), and protein concentrations were determined using standard curves obtained from serial dilutions of bovine serum albumin (Crystallized BSA Fraction V, Roche, Germany). Antibodies for HSP27, HSP70 and HSP90 were purchased from Cell Signaling, while GAPDH and beta-actin (B-actin) were purchased from Sigma. For a full list of antibodies and the concentrations used in western blot and Peggy Sue™, see appendix 2.

Protocol

Cells were treated as described in section 3.3 and incubated in T25 nuncleon flasks. After incubation, cell medium was transferred from each flask to a 50 ml centrifuge tube and cells were detached with 0.25% trypsin-EDTA. Cells were transferred to respective tubes by addition of PBS, centrifuged at 1000 g for 5 minutes and then transferred to eppendorf-tubes with PBS and centrifuged again at 1000 g for 5 minutes. Finally, supernatants were discarded and each cell pellet was stored at -20ºC for at least 24 hours prior to cell lysis.

To lyse the cells, frozen cell pellets were suspended in approximately 100 µL lysis-buffer. If cell pellets were large, more lysis buffer was added to ensure protein concentration within applicable range of the BCA-assay. After lysis buffer was added, cell samples were placed on ice and vortexed briefly every 10 minutes for approximately one hour. Samples were then sonicated 3 times with an Ultrasonic Homogenizer (4710 Series, Cole-Parmer Instrument Co.). To remove cellular debris from the lysates, samples were centrifuged at 13.000 rpm for 15 minutes at 4ºC and supernatants were transferred to clean eppendorf tubes. The enriched protein lysates were stored at –20ºC.

3.5.2 Bicinchoninic acid assay

The Microplate BCA™ Protein Assay Kit (ThermoFischer Scientific) was used to measure concentration of the protein lysates. Two reactions occur during the BCA-assay that allows analysis of protein concentration. The first reaction is the "biuret reaction", where peptides form a colored chelate-complex with copper (Cu^{2+}) from copper(II)sulfate in the reagent mixture. The second reaction is bicinchoninic acid (BCA) chelating reduced copper ions (Cu^{1+}) which are formed during the first reaction. Formation of colored BCA-copper complex during the second reaction amplifies signal intensity, which can be measured using a spectrophotometer. According to manufacturer, the signal correlates linearly with protein concentration over a range from 20 to 2000 µg/mL.

Protocol

Protein standards were made by diluting BSA in PBS to standards of 2000 -, 1500 -, 750 -, 500 -, 350 -, 250 -, 125 -, and 25 µg/mL protein. 20 µL of each protein standard were added in duplicate to a nuncleon™ 96-well plate. 3 µL of each lysate sample, as well as lysis-buffer, were then added in triplicate to the plate. Reagent A and reagent B from the BCA™ Protein Assay Kit were mixed in a 1:50 ratio, and 250 µL of the reaction mixture was added to each well. Plates were incubated for 30 minutes at 37ºC, and absorbance was read at 560 nm using Modulus Microplate reader. Standard curves from the protein standards were made in Excel.

3.5.3 Western blot Immunoassay

The western blot immunoassay is a well-established analytical technique for measuring expression of specific proteins in a mixed protein sample. Variations of the technique allow detection of both native and denatured proteins based on different properties, mainly size, charge and isoelectric point (pI). The technique can be divided into five main steps: (1) protein separation by gel electrophoresis, (2) protein transfer and immobilization on membrane, (3) incubation with primary antibody that binds protein of interest, (4) incubation with labeled secondary

antibody that bind the primary antibody, and (5) detection of labeled secondary antibody and signal analysis.

Western blotting is generally labor intensive, and each step in the western blot procedure may require modifications to allow optimal detection of a specific protein. During this study, western blotting was used to confirm the presence of heat shock proteins in cell lysates prior to Peggy Sue™ analysis. Antibody concentrations of HSP70, HSP27 and HSP90 were selected based on producer's recommendation. Proteins were separated based on size using NuPAGE ™ Novex 4-12% Bis-Tris Protein Gels (Thermo Scientific), which are pre-cast polyacrylamide gels used for size separation of proteins in reducing conditions. 4-12% denotes the amount of polyacrylamide within the stacking and separation matrix, respectively. Although the precast gels contain no sodium dodecyl sulfate (SDS), or its analog lithium dodecyl sulfate (LDS), it is added in sample- and running buffers.

The proteins were separated using sodium dodecyl sulfate polyacrylamide gel electrophoresis (SDS-PAGE). Prior to electrophoresis, protein lysates were mixed with the reducing agent dithiothreitol (DTT), which reduces disulfide bonds and unfolds the protein structure, as well as a sample buffer containing SDS. SDS/LDS are anionic detergents that denature and bind proteins, giving the proteins a net negative charge needed for separation by electrophoresis. Smaller proteins move faster through the polyacrylamide gel network, and protein samples are thereby separated by molecular size (kilodalton, kDa) during electrophoresis.

Protocol

Protein lysates were mixed with sample buffer (NuPAGE LDS Sample Buffer (4X); Invitrogen™), reducing agent (NuPAGE Sample Reducing Agent (10X); Invitrogen™) and distilled water to a 1 µg/uL protein solution. Samples were vortexed briefly and denatured at 95ºC for 10 minutes. 7 uL of See Blue Standard® Plus2 Pre-stained Protein Standard (Thermo Scientific) was added to the first SDS-PAGE well to allow protein size confirmation, and 15 µL of sample was added to respective wells.

Proteins were separated by electrophoresis using MES running buffer (buffer contents: see appendix 1) at 120V for 1 hour (BioRad PowerPac). For protein transfer, sponges were wetted in transfer buffer with 20% methanol (buffer contents: see appendix 1), and assembled in a "gel-membrane sandwich" together with the methanol-activated Polyvinylidene difluoride (PVDF) membrane (Invitrogen). The transfer sandwich was placed in the electrophoresis chamber (Invitrogen Novex® Mini-Cell) and transferred for 1 hour at 400 mA.

When protein transfer was complete, membranes were blocked for 1 hour at room temperature with 5% (w/v) dry-milk (Tine®, Norway) in Tris-buffered saline (TBS) with Tween 20® (T) (Millipore Sigma) on a plate mixer. Tween 20 is a detergent that prevents unwanted protein-protein interactions, and dry-milk protein is added to block non-specific protein binding and reduce background noise. Primary antibodies were diluted in 5% dry-milk TBS-T solution and incubated with membrane at 4ºC overnight. Next day the membrane was washed 3 times for 10 minutes with TBS-T and incubated with secondary antibody, which was diluted in 5% dry-milk TBS-T, for 1 hour at room temperature. The secondary antibody is conjugated to a Horseradish-Peroxidase (HRP), and was selected based on the primary antibody's animal of origin. HRP-conjugated antibodies targeting both mouse and rabbit were used (Dako, Agilent Technologies). After secondary antibody incubation, the membrane was washed again 3 times with TBS-T buffer.

Super Signal™ Western Plus Substrate (Thermo Fisher) was mixed according to manufacturer's instructions and added to the membrane. The mixture contains luminol, which is the substrate HRP uses to produce luminescence. Luminescence signal was detected and photographed using a G-BOX imaging system (Syngene), modified with Photoshop™ and analyzed with ImageJ™ software.

3.5.4 Peggy Sue Size immunoassay

Peggy Sue is one of several machines recently developed by Protein Simple™ (San Jose, CA). Peggy Sue performs automated semi-quantitative immunoassays based on the main principles of western blotting: separation, immobilization,

immunoprobing and indirect detection of target protein. On Peggy Sue, however, each step is performed within capillaries, which permits the use of less protein sample and antibody compared to traditional western. Being automated, the method also gives more accurate and consistent data.

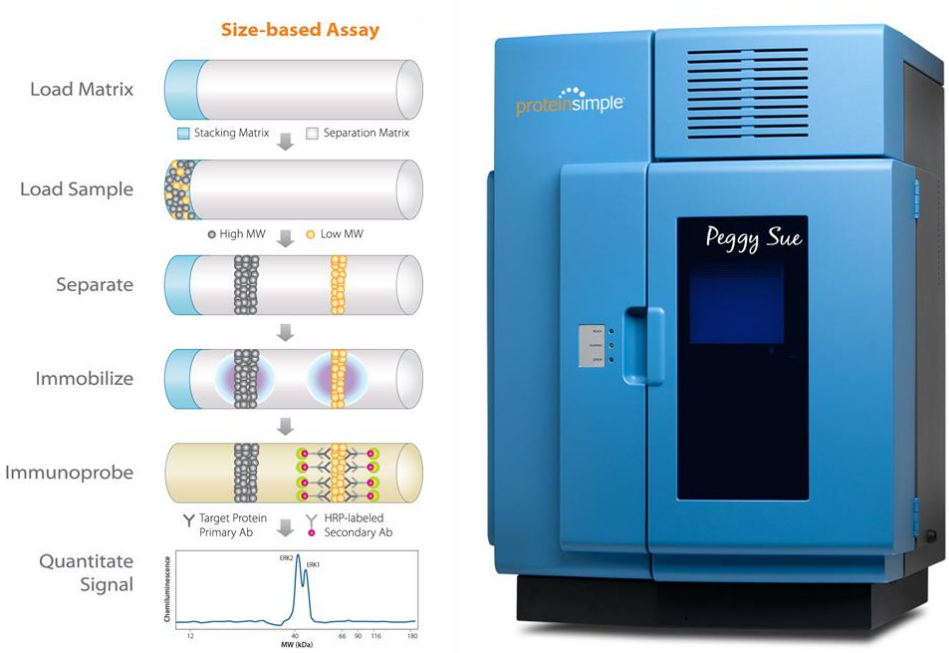

Figure 5: The individual steps of Peggy Sue immunoassay are fully automated (left) and processed by the Peggy Sue instrument from ProteinSimple (right). From the 'Sally Sue and Peggy Sue User Guide'. Modified from https://www.proteinsimple.com/simple_western_assays.html

The patented technology is based on a unique compound which is coated on the inside of the capillaries. The compound is activated by UV-light and covalently binds peptide chains, immobilizing proteins and allowing subsequent analysis to take place within the capillary itself (figure 5). It should be noted, however, that the binding process can disrupt an epitope normally accessible by an antibody on traditional western blot, and the technique requires optimization depending on the antibody used and the protein of interest.

Peggy Sue can analyze proteins based on both size and charge, but was only used during this study to analyze proteins based on size. The aim was to measure the expression patterns of HSP70 in the cell lines after treatment, to determine if its

expression could be linked to cell line treatment response. The house-keeping proteins B-actin and GAPDH were also analyzed to allow normalization of the signal between samples. Programming of Peggy Sue run and analysis of data was made using the Compass© software (ProteinSimple, version 2.7.1).

Protocol

Samples were prepared according to manufacturer's instructions using Peggy Sue or Sally Sue-Rabbit (12-230 kDa) Size Separation Master Kit (Protein Simple). Protein lysates were mixed with the contents of 'Standard Pack 1' (Protein Simple), which include DTT and a biotinylated ladder, and were denatured at 95°C for 5 minutes. 5 µl of sample was loaded per well on the 384-well microplate. The microplate was then loaded with biotinylated ladder, antibody dilutent, primary antibody, HRP-conjugated secondary antibody, stacking and separation matrix, and finally luminol-peroxide substrate mixture based on manufacturer's recommendations (figure 5). All reagents excluding primary antibodies were purchased from ProteinSimple™. The Compass software was used to program and start Peggy Sue analysis. The machine separated the proteins by capillary electrophoresis at 250V for 40 minutes, followed by incubation with primary and secondary antibody for 30 minutes each. All parameters required for Peggy Sue run were selected prior to analysis and based on manufacturer's recommendations for Peggy Sue Size separation 12-230 kDa.

Procedural changes were only made in the concentrations of protein lysate and primary antibody. The protein samples were diluted and run on Peggy Sue in concentrations ranging from 0.8 to 0.2 µg /µl, while antibody concentration of HSP70 and HSP27 was increased from 1:50 to 1:300 to optimize signal detection. All antibody concentrations are noted in appendix 2. Both concentration of protein lysate and primary antibody used are noted in the results.

3.6 Flow cytometry

Flow cytometry is a technique for analyzing individual cells as they flow in a liquid through a beam of light. When cells passes through the light, several sensors detect

light scattering and fluorescence, and register properties of the individual cell. The light signals are then converted to electronic signals that can be analyzed on a computer. This allows measurement of both physical properties of cells, including size and granularity, as well as fluorescence signal within the cell. Several wavelengths of fluorescence can be measured simultaneously and allow analysis of many components within a single sample. Cells can be analyzed by staining with fluorescent dyes that bind directly to the component(s) of interest, or through antibodies conjugated to a fluorescent dye. Cells are often 'fixated' prior to staining, as it prevents autolysis and degradation of cell components. Fixation also permeabilizes cellular membranes and allows dyes or antibodies to penetrate the cell.

Flow cytometry allows high-rate analysis of individual cells, and is a useful tool for investigating cell properties that cannot be detected by other methods, including viability assays. Although each cell that passes through the sensor is analyzed, data is commonly presented in fraction of the total number of cells analyzed. Flow cytometry was used during this master thesis to investigate the effects of treatment on cell cycle distribution and apoptosis. Analysis by flow cytometry was done in collaboration with Idun Dale Rein at the Flow Cytometry Core Facility (Cancer Research Institute, Radium Hospital, Norway).

Cell fixation protocol

Cells were treated as previously described and incubated in T25 nuncleon flasks. After 24 hours of incubation, cells were detached by trypsin-EDTA, washed with PBS, and centrifuged at 1700 g for 3 minutes. PBS was removed, and cell pellets were permeabilized by drop-wise addition of ice-cold methanol (VWR Chemicals). Cells were kept at - 20ºC for minimum 24 hours to ensure permeabilized cell membranes. In addition, one sample was extracted prior to treatment (at 0 hours), fixated as described above and stained together with samples from the same experiment.

3.6.1 TUNEL assay

Terminal deoxynucleotidyl transferase (TdT) dUTP Nick-End Labeling (TUNEL) assay is used to detect apoptotic cells by incorporation of labeled nucleotides by TdT enzymes. Cells that undergo apoptosis activate endonucleases that degrade and form 'nicks' within DNA. These 'nicks' within the DNA strand can be filled in with labeled nucleotides by TdT enzymes. The TUNEL assay uses dioxyuridine Triphosphate (dUTP) molecules conjugated to biotin as substrate for the TdT enzyme. If the biotinylated UTP is incorporated into the DNA of a cell, it can be detected by addition of labeled-streptavidin, which has a high specific affinity for biotin. The labeled streptavidin used for TUNEL assay contained cyanine 5 (Cy5) – which emits fluorescent light at peak 650 nm.

Protocol

Prior to staining, fixated cells were transferred to 5 mL Falcon® round-bottom polystyrene test tubes (Corning Inc.) and washed with PBS. The TUNEL-assay reaction mixture was prepared according to manufacturer, and 40 µl of the mixture was added to each sample which were incubated at 37ºC for 30 minutes. 3 ml of PBS was then added to each sample, and the samples were centrifuged at 1000 g for 3 minutes and the PBS was removed by pipette. Dry milk was mixed with PBS to a 5% weight/volume ratio and centrifuged at 2000 g for 3 minutes. The supernatant was used to dilute the Cy5-labeled streptavidin to a 1:400 concentration. 100µL of the solution containing streptavidin (1:400) was then added to each sample, and the samples were covered in aluminum foil and incubated for 40 minutes. 3 mL PBS was added after incubation, samples were centrifuged at 1700 g for 3 minutes, and PBS was removed. Finally, samples were stained with Hoechst before flow cytometry analysis.

3.6.2 Cell cycle analysis

Analyzing cell cycle distribution can be useful for investigating cellular changes that occur after a specific treatment. Cell cycle analysis is based on the principle that cells replicate their DNA as they move through the cycle. When DNA is replicated

the total amount of DNA within a cell increases from n to 2n, which can be measured and used to analyze the distribution of cells within the G1-, S- and G_2/M-phase by flow cytometry. In this study, cells were stained with Hoechst 33258 (Invitrogen) to determine the cell cycle distribution of cells after treatment. Hoechst is a nucleic acid stain that binds double-stranded DNA and emits blue fluorescence that can be detected by flow cytometry.

Protocol

Prior to staining, fixated cells were transferred to 15 mL round-bottom centrifuge tubes and washed with PBS. For convenience, samples were always stained by TUNEL-assay before Hoechst. Hoechst 33258 was diluted in PBS (1:400) and 300-600 µL was added to each cell pellet, depending on the amount of cells present. Samples were kept at 4ºC overnight before flow cytometry analysis. Before flow cytometry, cell samples were passed through the Falcon® cell strainer cap (Corning Inc.).

3.6.3 Flow cytometry: gating strategy and data analysis

Analysis of flow cytometry data was done with the FlowJo™ software. Regardless of staining method, gating is required to exclude any aggregated or fragmented cells to allow analysis of single, stained cells. For this study, the Hoechst DNA stain was used to gate for single cells within each sample by including only cells with a cell-volume (area) which corresponded to the single-celled population (figure 5A). Further analysis was then made within the single cell population. When single cells had been gated, apoptosis and cell-cycle analysis could follow. TUNEL- analysis was made by creating gates around cells with little or no Cy5 stain (figure 5B).

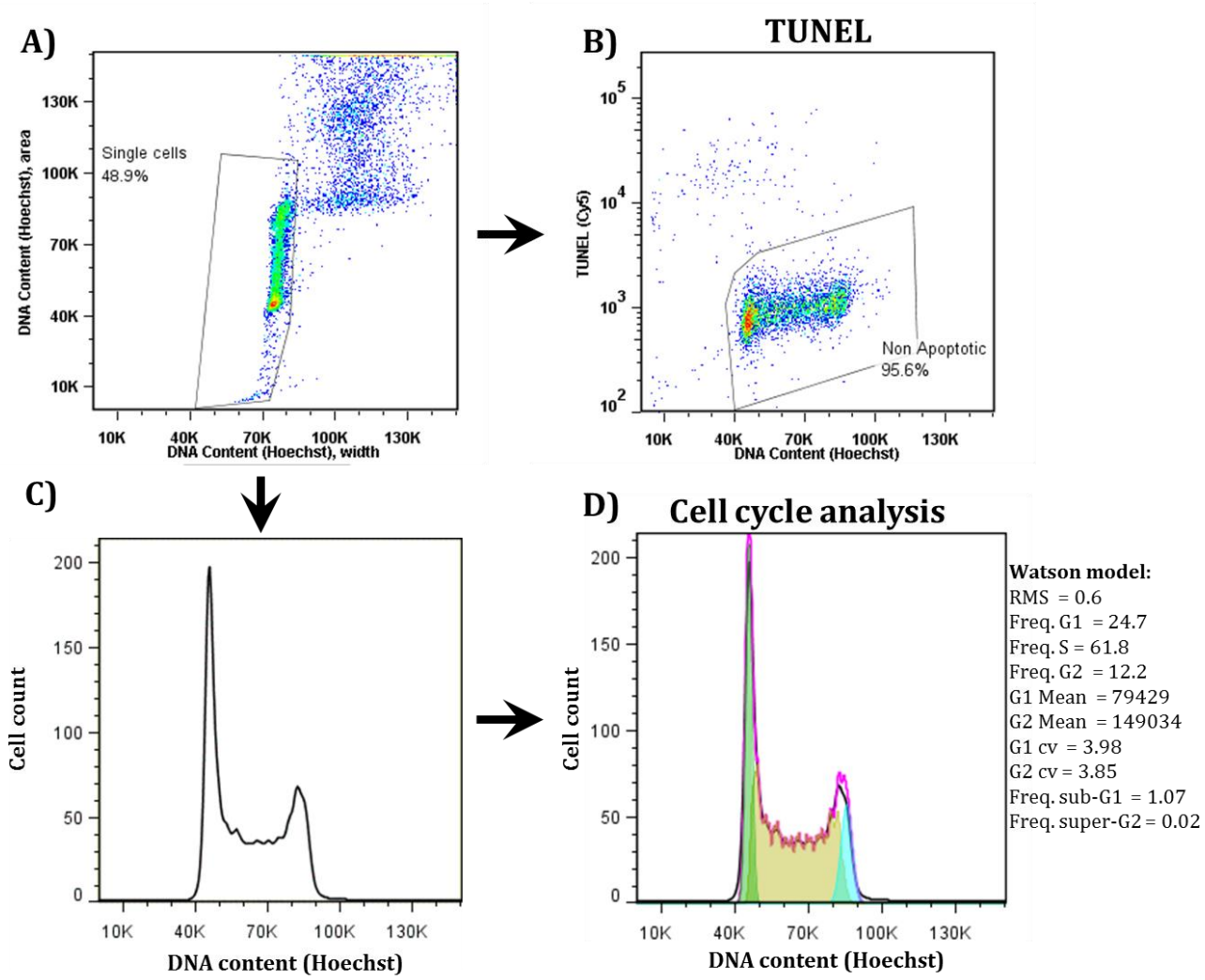

Figure 6: Gating strategy of B76 cells stained by Hoechst and TUNEL after flow cytometry. **A)** Gating of single cells within the total sample removes unwanted doublets, **B)** analyzing single cells by Cy5 staining from TUNEL assay is used to estimate the non-apoptotic/apoptotic fraction within the sample, **C)** Histogram of the single-celled population by DNA content, **D)** Cell cycle distribution as analyzed in FlowJo using the 'Watson' algorithm.

Although this method is less accurate, consistent gating increases precision and gives good indication of apoptotic fractions within each sample. The fraction of apoptotic cells shown within the single-cell observations in figure 6A, for instance, was estimated to be 4.4 % (figure 6B). Cell cycle analysis of Hoechst stained cells was done using the integrated cell-cycle analysis tool in FlowJo. The cycle distribution is calculated by a Watson 'pragmatic' algorithm which estimates the fraction of cells in G1 and G2/M-phase. The model assumes a normal distribution of

cells within the G1 and G2 phase, and uses these values to estimate the frequency of cells in S-phase. Cell cycle analysis may require optimization if samples contain noise or have broad G1 and G2 peaks. The model 'fit' is reported as root mean square (RMS), where RMS values <1.5 are generally considered as 'good' fit.

3.7 Ugelstad beads: antibody-conjugated magnetic beads

Ugelstad beads (Dynabeads) are magnetic nanoparticles which can be modified with ligands or antibodies to bind specific molecules on the cell surface. The immunomagnetic Dynabeads M450 (Invitrogen, Oslo, Norway), were coated with the MOC31 antibody as previously described [73]. The MOC31 antibody target EpCAM, and can be added to small tissue or cell suspensions where binding of magnetic beads to EpCAM-positive cells allow manipulation under a magnetic field, including separation of positive cells in cell mixtures (figure 7).

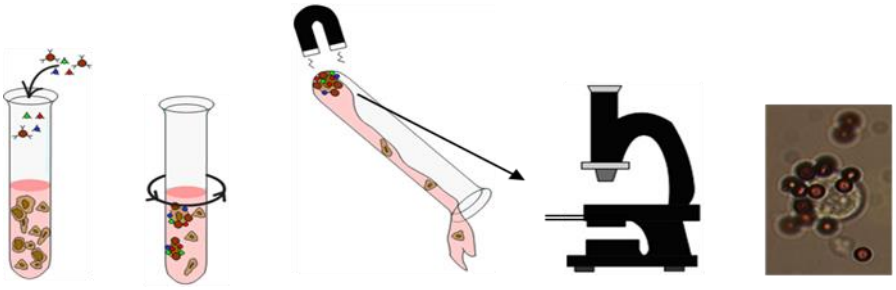

Figure 7: Ugelstad beads bind EpCAM and allow isolation and detection of EpCAM-positive cells.

For this study, Ugelstad beads where used to confirm the presence of EpCAM on the surface of the cancer cell lines. EpCAM is the target for MOC31PE. Positive staining with Ugelstad beads was a simple method for determining if cell lines would be susceptible to MOC31PE treatment.

Protocol

Cells were detached from culture flasks with 0.25% trypsin-EDTA, centrifuged and suspended in PBS. 10 uL Ugelstad bead solution (15 mg beads/ml) was then added to the cell samples (1 million cells/ml), in addition to vehicle solution containing nickel-beads only, and incubated on mixing wheel for 30 minutes at 4ºC. Later, each

sample was transferred to respective glass-covers/slits and viewed under a light microscope to confirm the presence of EpCAM.

3.8 DNA sequencing

DNA sequencing is the process of analyzing the specific order of nucleotides in DNA. Sequencing in cancer research often consists of determining specific alleles in cancer-related genes, as it is less time-consuming and cheaper than sequencing large DNA segments or whole-genome sequencing. Ion-torrent sequencing was used to determine if the cell lines pmOC8, B76 and OVCA433 possessed mutated alleles in cancer-related genes. Ion AmpliSeq™ Cancer Hotspot Panel v2 (Fischer Scientific) was used to amplify segments for 50 cancer-related genes. After amplification, samples were run on an Ion torrent sequencing platform.

DNA isolation protocol

Cells were detached from flasks using 0.25% trypsin-EDTA and washed twice in PBS. The DNA-isolation kit Nucleospin® tissue (Macherey-Nagel) was used to purify DNA from cell samples. Cells were lysed at 95ºC in a solution containing SDS, before adding 70% ethanol and binding buffer (containing chaotropic ions) to enable reversible DNA binding to the silica membrane located in the NucleoSpin® columns. Contaminants were removed by addition of wash buffers (Macherey-Nagel) before DNA was eluted with deionized dH_2O and stored at -20ºC.

The purity and concentration of the DNA samples was determined by spectrophotometric analysis using a NanoDrop 2000 UV-spectrophotometer (Thermo Scientific). The ratio of absorbance at 260 nm to 280 nm determined the amount of contaminants, and a value over 1.80 was considered sufficiently pure for DNA sequencing.

DNA sequencing was done in collaboration with Annette T. Kristensen at our department. Purified DNA-samples from B76, OVCA433 and pmMOC8 were sequenced by Ion Torrent platform (Thermo Fisher Scientific). Sequencing data was processed by biobanking strategist Christin Lund-Andersen at our department.

3.9 Animal models

During this master thesis, the cell lines B76 and OVCA433 were used in an attempt to establish an animal model for HGSOC peritoneal metastases (PM). All experiments involving animals were approved by The National Animal Research Authority and carried out according to regulations posed by the European Convention for the Protection of Vertebrate Animals used for Experimental and Other Scientific Purposes (ETS No.123). Female mice (Athymic Nude-Foxn1^{nu}) were kept under pathogen-free conditions, and food and water were supplied ad libitum, supplemented with 17-ß-estradiol (4 mg/l).

Protocol

Cells were detached from culture flasks with 0.25% trypsin-EDTA, centrifuged at 1000 g for 5 minutes and suspended in medium without FBS. Cells were counted manually, and 2.5 million cells were injected intraperitoneally into female Nude-mice. The well-being of the mice was carefully monitored throughout the experiment, and animals were sacrificed by cervical dislocation on day 4, 7 and 11, or when signs of disease and/or weight loss exceeded 15%. At autopsy, metastatic lesions and nodules were collected and weighed. Tumor tissues were then formalin fixed, paraffin-embedded, sectioned and stained with haematoxylin-eosin (H&E). Animal experiments were done in collaboration with Stein Waagene at our department, and my supervisor Dr. Andersson.

3.10 Data analysis

Data obtained from MTS and ATP assays were analyzed using Microsoft Excel™. First, the average signal for each treatment was calculated from triplicate wells. The average background signal, measured as medium only, was then subtracted from each sample including control. Viability was calculated by dividing the average signal from treated samples with the average signal from untreated control (cell suspension containing medium only, incubated at 37ºC). The relative viability obtained from treated samples was expressed as percentage of the 37ºC control. Average viability from three biological replicates was then plotted as a line graph

using Excel™, and standard deviation error-bars were added. Experiments without three biological replicates were marked in the figure subtext; for these figures the average and standard deviation of a single replicate are shown instead.

A t-test was used to analyze differences in viability between samples treated at 37ºC compared to 42ºC, at identical drug concentrations. Statistical analysis of the viability data was made using Analysis ToolPak in Excel™. Using a two-tailed paired t-test for means, the statistical cutoff value was set to $p<0.05$ and statistical significance is indicated with asterisk: * = $p<0.05$, ** = $p<0.01$.

For data obtained from flow cytometry, western blot or PeggySue™, data was analyzed using appropriate software described under respective segments. For these methods, no further statistical analysis was made due to lack of biological replicates.

4 Results

The following section contains the results obtained during the study, which are divided into 5 main segments: (1) establishing an in vitro model mimicking the HIPEC procedure and preliminary cell-line studies, (2) cell viability results obtained from the in vitro HIPEC-model, (3) TUNEL and cell-cycle analysis, (4) protein expression analysis, and (5) cell viability results obtained from treatments with MOC31PE using the in vitro HIPEC-model. All experimental figures represent triplicate datasets from three biological replicates unless otherwise noted. Error bars show standard deviation, and statistical significance is marked with asterisk as described in section 3.10.

4.1 Establishing an in vitro HIPEC model

At the core of this study lies HIPEC, a treatment procedure where cancer cells are exposed to a combination of HT and chemotherapy for short durations. To investigate the response of cancer cell lines to this treatment, we set out to establish an in vitro model that mimicked the conditions of clinical HIPEC.

During early attempts, cell lines were treated in 96-well plates covered in parafilm and incubated on water baths set to 37ºC or 42ºC for both 30 and 90 minutes. The main issue was the high rate of evaporation, leading to droplet formation on plate lids and posing a possible contamination concern due to the chemotherapy drugs involved. Removing the chemotherapy solution after the treatment had ended, which is relevant for HIPEC, was difficult and resulted in variation between individual triplicates.

We chose to replace the 96-well plates with 15 ml plastic centrifuge tubes. The rate of evaporation was no longer a concern and tube caps prevented contamination of the water baths. Removing the chemotherapy-medium mixture from cells after centrifugation was significantly easier, and because cells could be seeded onto 96-well plates after treatment instead of before, less variation was observed between individual triplicates. However, treatment occasionally resulted in near-complete

loss of viability, regardless of drug concentration. We discovered the temperature of the hyperthermic water bath (an immersion circulator) to fluctuate and frequently reach above 42ºC, causing increased cell death. The problem was solved by replacing the immersion circulator with a high-precision (±0.2ºC) temperature controlled water bath (SUB Aqua Pro; Grant Instruments, Cambridge).

While treatment temperature now was precise, we noticed that the dose-dependent response of cells was largely inconsistent, and we hypothesized that the variation arose from incomplete removal of the drug-medium solution from cells after treatment. By adding a washing step after removal of drug-medium solution, the dose-dependent response became consistent between experiments and variation within triplicates improved. While treatment for both 30 and 90 minutes was attempted initially, reduction in viability observed by MTS measurements after 30 minutes treatment with cisplatin and mitomycin was low (data not included). Instead of attempting to include two treatment durations, 90 minutes was selected as it closely resembles the clinical duration of HIPEC.

The established in vitro model successfully mimicked the conditions of HIPEC; with short exposure of cells to drug and HT, as well as "complete" removal of chemotherapy drugs after treatment, consistent viability measurements were obtained. The established model was used to investigate the effect of HT during HIPEC, by incorporating a small panel of cell lines representing HGSOC.

4.2 Preliminary analysis of the ovarian cancer cell lines

Genotypic data for the cell lines were gathered from recent published articles and the COSMIC database (The Catalogue of Somatic Mutations in Cancer). The presence of relevant mutations for OC, including TP53, was compiled and can be seen in table 2. No relevant or otherwise unreported mutations were discovered during the sequencing of B76, pmOC8 and OVCA433. However, all cell lines, including the novel primary cell line pmOC8, were found to be of HGSOC origin (by Patologist Ben Davidson, The Radium Hospital). The morphology of each cell line was notably different; B76 grew in a tight cobblestone-like pattern, while OVCA433

had an elongated phenotype making it appear larger in size (fig. 8). OVCA432 had the highest growth rate of the cell lines.

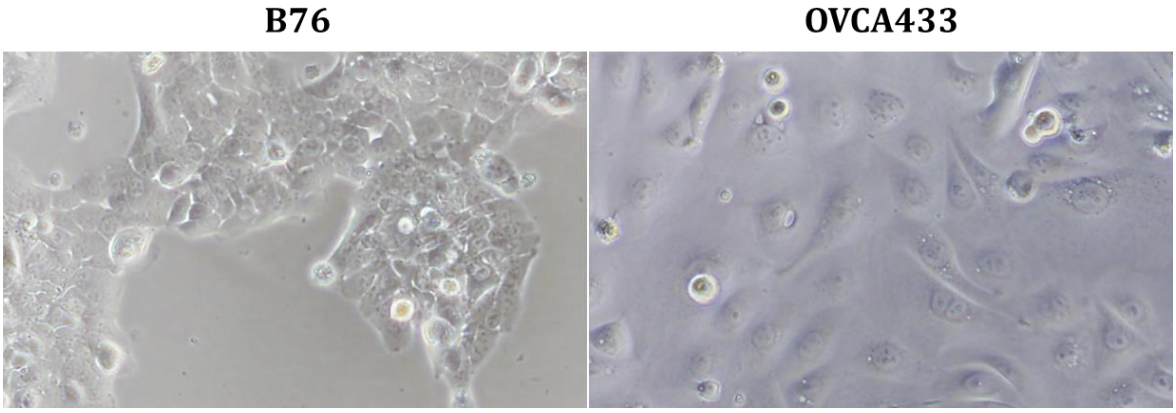

Figure 8: The cell lines B76 and OVCA433 show distinct morphology; while B76 is tightly-packed, OVCA433 has an elongated phenotype. Pictures taken at 400X magnification.

While OVCA433, OVCA432 and CaOV3 were able to form colonies even at low seeding densities, B76 appeared to be contact-dependent, which prevented use of colony-formation assay.

Table 2: Overview of cell lines and relevant mutations

Cell line	TP53	Others
B76	Mutated	PIK3CA
OVCA433	Wild-type [78]	CDKN2A[79], BRCA1/2 [80], EPCAM, HSPA1A (HSP701a), PARP12
pmOC8	Mutated	BRCA1 (unpublished)
OVCA432	Mutated [81]	BRCA1/2 [80], ATP1A1, HSPA1L (HSP701), ATP10B, ATM
CaOV3	Mutated [82]	VEGFC, EGFR, MAP2K1/3K1

4.2.1 Establishing intraperitoneal metastases in a mouse model

Cell lines B76 and OVCA433 were transferred to nude mice by intraperitoneal injection, to determine their capability to form pertitoneal metastases. B76 had a 100% 'take rate' and formed tumors which increased in size over time. The mean survival time (MST) after injection was 24 days (SD 1.0). Tumors were mainly found on the mesentery lining of the intestines (fig. 9), as well as on the greater omentum, the pancreas, the kidney and the spleen.

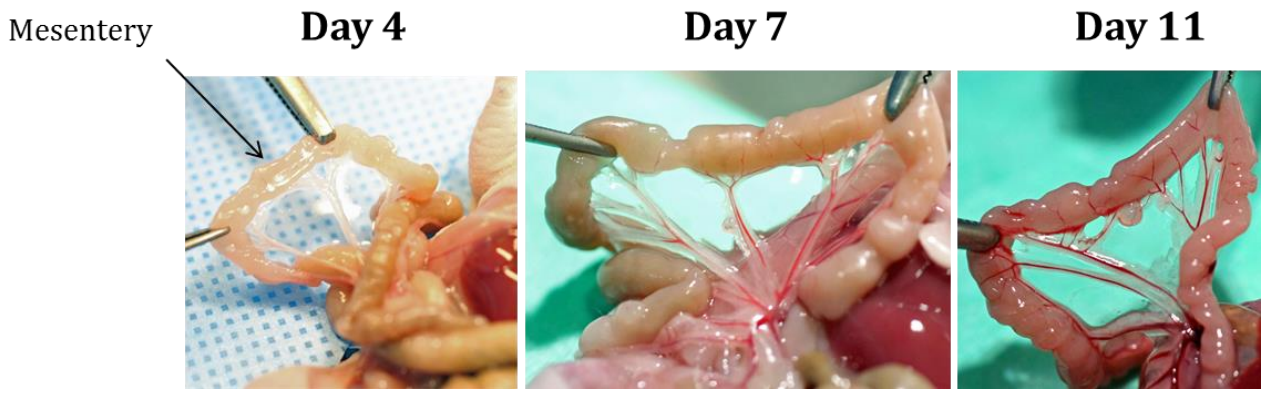

Figure 9: Tumors formed on the mesentery of mice injected IP with B76 cancer cells after 4, 7 and 11 days. By holding the colon with metallic tweezers, mesentery and tumor nodules present are made visible. Note the size of the nodule in "Day 7" (middle) compared to the nodule at "Day 11" (right).

The tumor marker profile and morphological characteristics of B76 were suggestive of HGSOC, and compatible with the original patient's tumor tissue according to pathologist Dr. Davidson and my supervisor Dr. Andersson. The OVCA433 cell line failed to cause tumor formation (n=2), and unsuccessful attempts have been reported previously [83].

4.3 Cell viability analysis by MTS assay

To determine the dose-response relationship of cisplatin, carboplatin and mitomycin, two cell lines were selected for analysis. B76 had been studied previously at the department [84], and was therefore selected together with OVCA433, which possesses wild-type TP53 [78]. These two cell lines were treated with several concentrations centered on the clinical HIPEC dose of selected drugs. The aim was to determine if HT (42ºC) affected the dose-response relationship seen at normothermia (37ºC). As ATP assay was found to correlate strongly with MTS assay (see appendix 4), the viability data presented in the following sections will only include data obtained from MTS assays.

4.3.1 Cisplatin

Cisplatin is the backbone of conventional chemotherapy of OC. To determine the response of B76 and OVCA433 to cisplatin, the two cell lines were treated as

previously described (section 3.2.1) with four cisplatin concentrations ranging from 37.5 to 300 μM. After 72 hours incubation, viability was assessed with MTS assay.

The cell lines had strikingly different responses to HT (fig. 10). B76 showed a dose-dependent loss of viability, but did not appear sensitive to 90 minute treatment with cisplatin at clinical HIPEC concentration (75 μM). When treated in combination with HT, however, viability dropped dramatically; the lowest concentration of cisplatin at 42ºC yielded nearly the same viability reduction as the highest concentration used at 37ºC (fig. 10A). Indeed, the half maximal inhibitory concentration (IC50) of cisplatin was over 150 μM at 37ºC, but achieved at already 37.5 μM in combination with HT.

In contrast, HT did not sensitize OVCA433 to cisplatin. Although the dose-dependent loss of viability of OVCA433 resembled that of B76 at 37ºC, no decrease in viability was observed from combination treatment at 42ºC (fig. 10B). It also appeared to be less affected by HT alone (control).

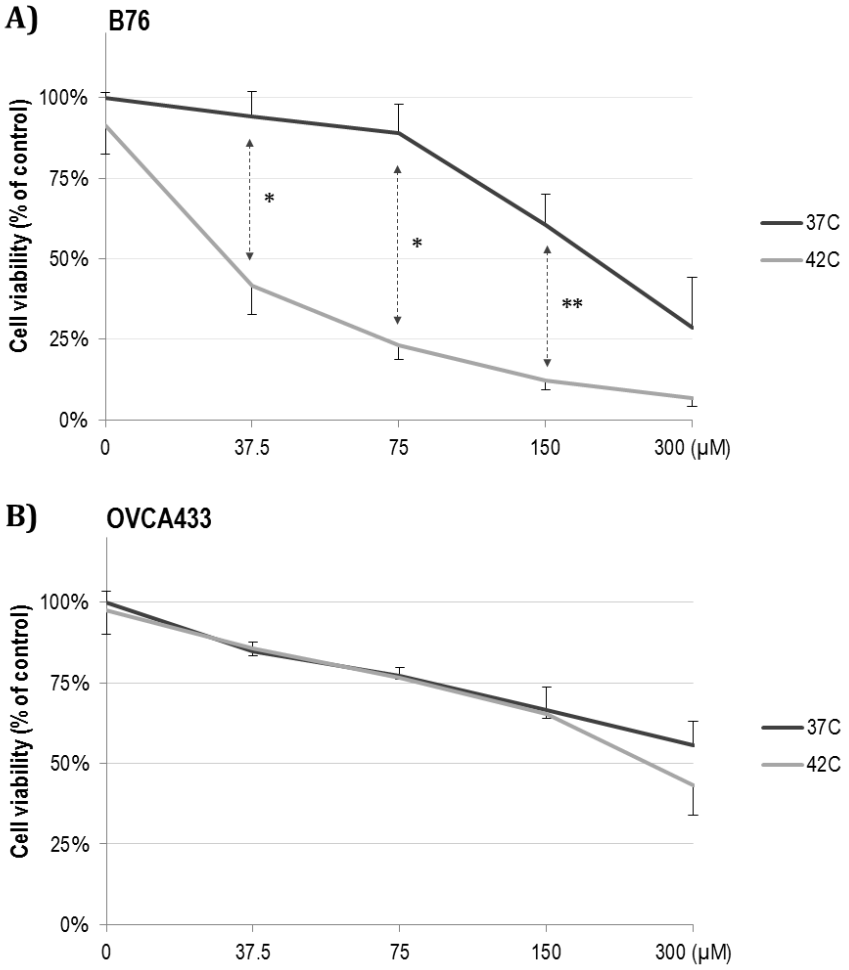

Figure 10: Viability measured 72 hours after treatment with cisplatin by MTS assay. **A)** B76 was not sensitive to cisplatin at clinical concentration (75 µM) when administered at 37°C; however, B76 viability was significantly reduced in combination with HT (42°C). **B)** OVCA433 was not, in contrast to B76, sensitized by HT, and appeared to respond to cisplatin in a dose-dependent manner.

4.3.2 Carboplatin

The cisplatin-analogue carboplatin has emerged as a candidate for HIPEC treatment. Clinical trials on intravenous (i.v.) carboplatin have shown similar survival outcome to that of cisplatin, and carboplatin has a favorable toxicity profile [85]. The clinical HIPEC concentration of carboplatin was estimated to be 250 µM, and cell lines B76 and OVCA433 were treated with three concentrations of carboplatin ranging from 125 µM to 500 µM.

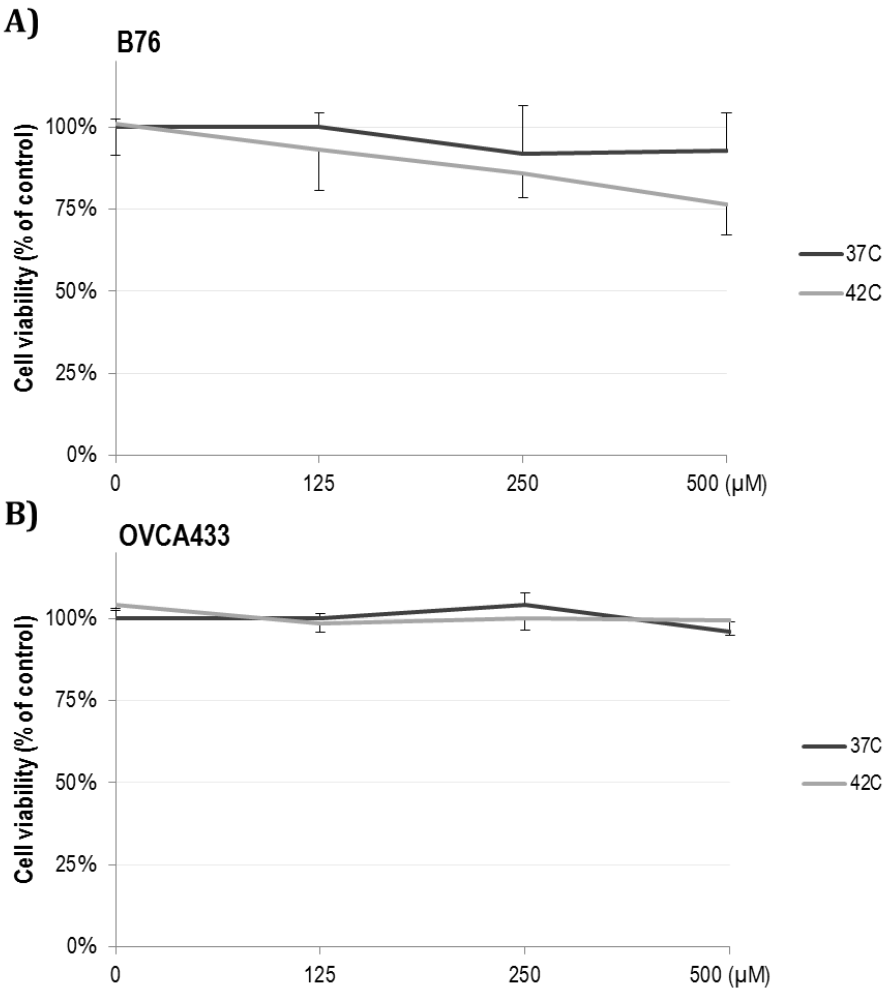

Figure 11: Viability measured 72 hours after treatment with carboplatin by MTS assay. **A)** Neither B76 nor **B)** OVCA433 were sensitive to carboplatin at clinical concentration (~250 µM**)**, and no significant effect was observed from treatment combination with HT. It is possible that the duration of the treatment (90 minutes) limits the uptake of carboplatin. Only one biological replicate was completed with OVCA433.

Both B76 and OVCA433 appeared to be resistant to carboplatin based on viability read-outs (fig. 11), and 90 minute treatment did not cause significant reduction in cell viability at the clinical concentration (250 µM). In contrast to the results from treatment with cisplatin, B76 was not sensitized to carboplatin by HT. As the response of OVCA433 indicated carboplatin resistance, only one biological replicate was completed with this cell line.

4.3.3 Mitomycin

While mitomycin has mainly been used in IP treatment of metastatic colorectal cancer (CRC), it has recently undergone clinical HIPEC trials for OC [86, 87]. The reported clinical HIPEC perfusate concentrations of mitomycin vary, and range from 20 – 60 μM [88]. We investigated the effect of mitomycin on B76 and OVCA433 in HIPEC conditions by treating the cell lines with mitomycin concentrations ranging from 30 μM to 120 μM.

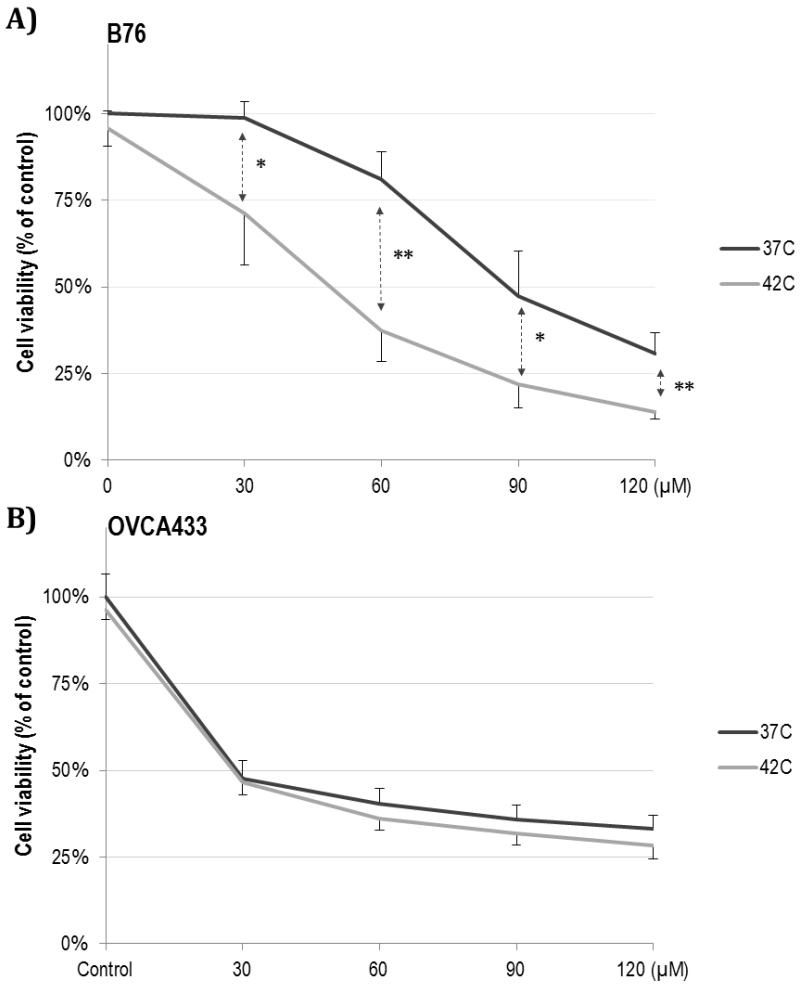

Figure 12: Viability measured 72 hours after treatment with mitomycin by MTS assay. **A)** B76 viability followed a dose-dependent pattern at 37ºC, however, HT significantly reduced the viability of B76 at all concentrations tested. **B)** While OVCA433 appeared sensitive to mitomycin at the lowest concentration, increasing the concentrations past 30 μM only marginally affected viability. Unlike B76, OVCA433 was not sensitized to mitomycin by HT.

The B76 cell line responded to mitomycin in a dose-dependent manner (fig. 12), but the loss in viability of B76 was again significantly increased in combination with HT. IC50 for mitomycin was near 90 μM at 37ºC, but decreased to less than 60 μM in combination with HT for B76 (fig. 12A).

On the other hand, OVCA433 did not appear to respond in a dose-dependent manner. The viability of OVCA433 was reduced to less than 50% of the control at 30 μM (fig. 12B). Concentrations beyond 30 μM had little impact on the viability in OVCA433, and viability decreased only an additional 25% after a four-fold increase in concentration (30 μM to 120 μM). While it is possible that a subpopulation of OVCA433 displayed higher resistance to mitomycin, which would explain early drop in viability but no significant decrease at higher dosage, it is also possible that viability measurements after 72 hours are too early to capture the response to mitomycin.

4.4 Cell viability screening of CaOV3, OVCA432 and pmOC8

The results from the viability assessment of cell lines B76 and OVCA433 were interesting. In sharp contrast to OVCA433, B76 was sensitized to cisplatin and mitomycin in combination with HT. Both cell lines appeared resistant to carboplatin, which is currently a candidate drug for HIPEC at the Radium Hospital (Clinical trial planned to start 2017). The results pointed to a fundamental question considering HIPEC; does HT in all cases benefit HIPEC?

Viability measurements of B76 and OVCA433 indicated a cell-line specific response to combination treatment, as well as a drug-dependent sensitization by HT. We set out to determine if other cell lines responded similarly to either B76 or OVCA433 by selecting a small panel of cell lines for combination treatment. The selected HGSOC cell lines were OVCA432, CaOV3 and the novel cell line pmOC8, all containing the HGSOC 'trademark' of mutated TP53. These three cell lines were treated with a single drug dose at clinical concentration, and viability was assessed after 72 hour incubation as previously described.

4.4.1 OVCA432

The OVCA432 cell line appeared to have high resistance to all drugs at clinical concentration (fig. 13). While viability is decreased by HT during cisplatin treatment, the effect was not statistically significant (p = 0.06).

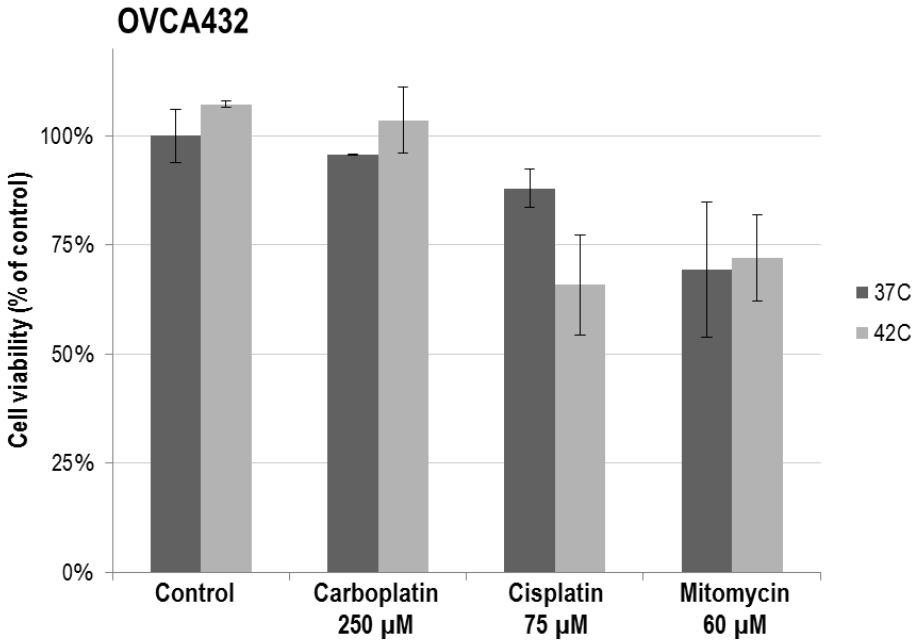

Figure 13: Viability of OVCA432 measured by MTS assay 72 hours after combination treatment. No large decrease in viability was observed for any of the three drugs at clinical concentrations. While HT appears to decrease viability of OVCA432 in combination with cisplatin, this effect was not statistically significant (p=0.06).

4.4.2 PMOC8

The recently established cell line pmOC8 responded to clinical concentrations of mitomycin (60 µM) with similar loss of viability as OVCA433 (fig. 13). Initially, it appeared that viability of pmOC8 was significantly reduced in combination treatment for cisplatin (fig. 14). However, while difference in viability for cisplatin treatment at 37ºC and 42ºC is statistically significant, a similar gap in viability was seen for the control samples. It is possible that the decrease in viability seen with all drugs tested is simply an additive cytotoxicity of HT in pmOC8 (see 42ºC control, fig. 14). As with OVCA432, pmOC8 was resistant to carboplatin.

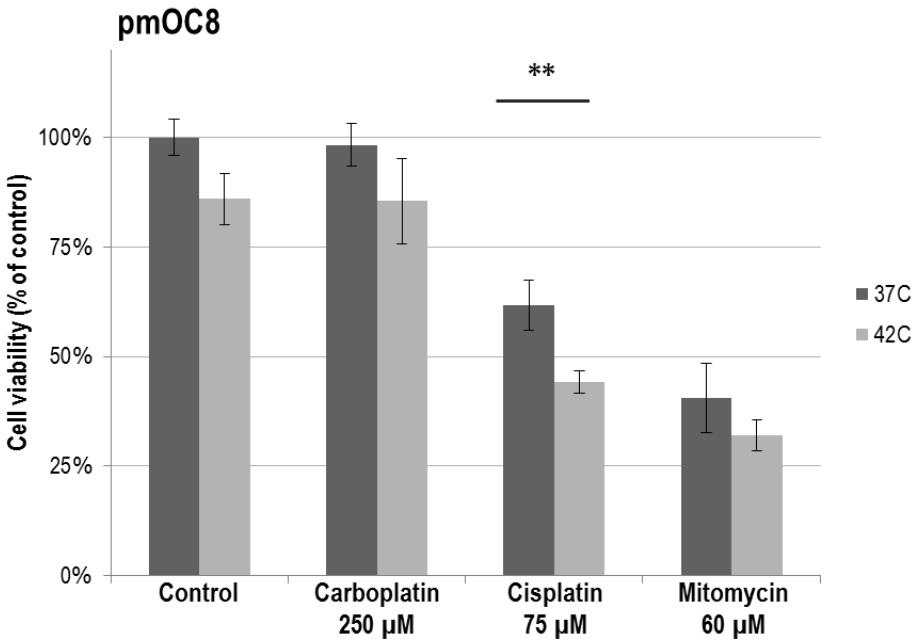

Figure 14: Viability of pmOC8 measured by MTS assay 72 hours after combination treatment. The patient-derived primary cell line pmOC8 is sensitive to cisplatin and mitomycin, and show potentiating effect of cisplatin in combination with HT.

4.4.3 CaOV3

The last cell line in the panel, CaOV3, is one of the most frequently used cell line model for HGSOC [82]. Similarly to the rest of the cell line panel, CaOV3 appeared to be resistant to carboplatin at clinical concentrations (fig. 15). CaOV3 was, however, hypersensitive to mitomycin at clinical concentration. Sensitizing effects of HT could not be observed for mitomycin as viability approached 0%. The sensitizing effect of HT to cisplatin treatment was evident in CaOV3, but only two biological replicates of the experiment were completed. By analyzing triplicate data sets from each biological replicate, the effect of HT on cisplatin was found to be statistically significant ($p=0.02$, $p=0.0003$, respectively).

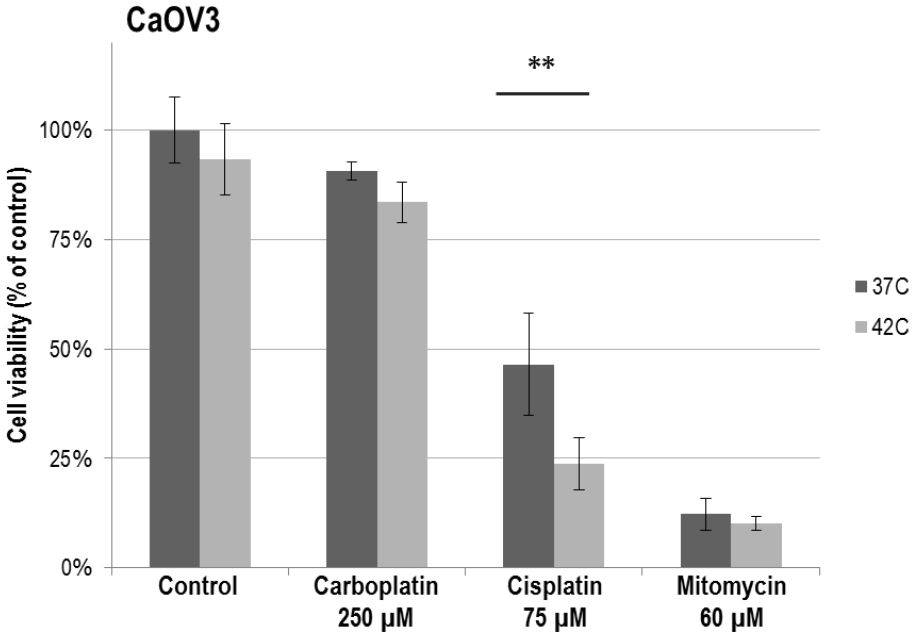

Figure 15: Viability of CaOV3 measured by MTS assay 72 hours after combination treatment. CaOV3 is sensitive to cisplatin and hypersensitive to mitomycin at clinical concentrations. As only 2 biological replicates were completed, statistical analysis was completed on single replicates instead.

4.5 Determining the effect of treatment on cell cycle distribution and apoptosis

The results from viability assessment of treated cell lines revealed large variations within the cell line panel. Notably, HT appeared to sensitize B76 in treatment with mitomycin and cisplatin. In contrast, viability of OVCA433 was not affected by HT under any treatment, and the cell line appeared to be non-responsive to HT. OVCA432 appeared most resistant to drugs tested at clinical concentrations, while CaOV3 was hypersensitive to mitomycin and sensitized to cisplatin in combination with HT (fig. 15). Determining the cell cycle distribution and rate of apoptosis within cell lines 24 hours after treatment could help explain the cell-line specific response to combination treatment.

4.5.1 Cell cycle distribution and apoptosis in pmoc8, B76 and OVCA433 after combination treatment

Cell lines pmOC8, B76 and OVCA433 were fixated both prior to treatment (marked 0 hours), as well as 24 h after treatment. Cells were stained with Hoechst and TUNEL for cell cycle and apoptosis analysis, respectively. Figures represent one biological replicate for pmOC8 and OVCA433, and two replicates for B76.

The highest rate of apoptosis caused by HT alone was found in the B76 cell line, with 27% apoptotic cells 24 h after treatment compared to only 4% in the control (fig. 16A). The other cell lines pmOC8 and OVCA433 had only 13%, but OVCA433 had equal frequency of apoptotic cells in the control independent of temperature (fig. 16C/D). For cisplatin, B76 cells treated at 37ºC had higher fraction in S-phase and 11% apoptosis after 24 hours. However, cisplatin and HT in combination resulted in smaller fraction in S-phase and 37% apoptosis, up 10% from HT alone (fig. 16A). For mitomycin, the fraction of apoptotic cells were 17% and 28% for samples treated at 37ºC and 42ºC, respectively. As such, no net increase in apoptosis could be seen based on 42ºC control. We also included carboplatin, and to our surprise, while no increase in apoptosis were seen at normal temperature, HT caused an increase in apoptosis to 32%, up 5% from HT alone. For B76, a trend was seen; the fraction of cells in S-phase was smaller for HT treated samples compared to samples treated at 37ºC.

For pmOC8, HT alone resulted in 13% apoptosis at 24 h after treatment, compared to 3% in the control (fig. 16B). For pmOC8, cells treated with HT in combination with cisplatin or mitomycin had lesser fraction of cells in S-phase compared to treatment at 37ºC (fig. 16B). The amount of apoptotic cells for cisplatin was however equal at both temperatures, but comparing the values to the control samples (3% for 37ºC control, 13% for HT), treatment at 37ºC appeared to cause more apoptosis at 24 hours after treatment. The same effect could be seen for mitomycin; 31% apoptosis were found in the sample treated at 37ºC but only 26% in combination with HT.

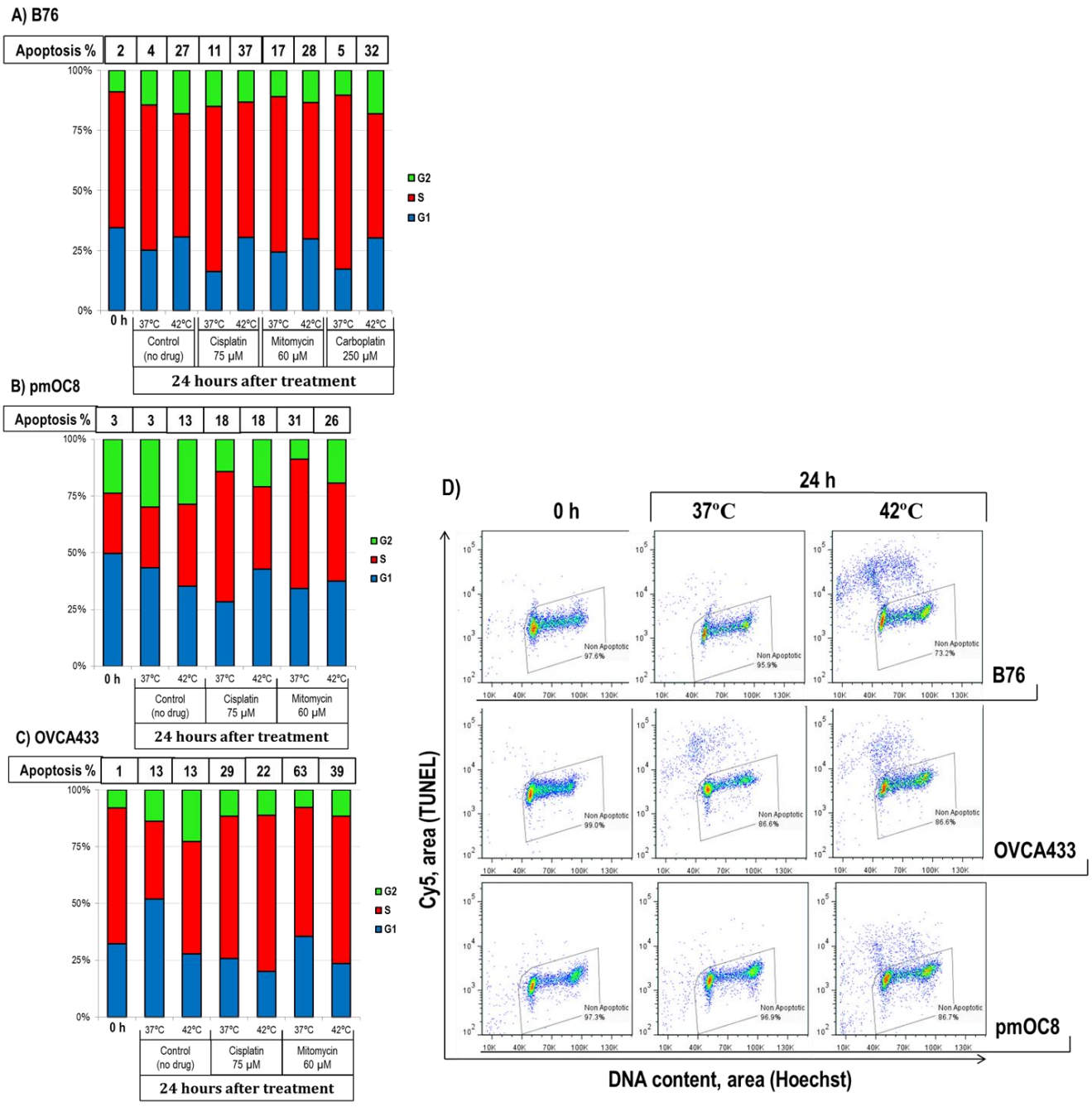

Figure 16: Summary of apoptosis and cell cycle distribution observed in cell lines after flow cytometry, **A)** B76, the only cell line were carboplatin treated samples were included, **B)** pmOC8, and **C)** OVCA433. Figure **D)** shows the apoptosis frequency in control samples for the three cell lines, prior to treatment (0 h) and 24 hours after treatment. Note the high fraction of apoptotic cells in B76, and the thermo-tolerant behavior of OVCA433.

Both pmOC8 and B76 displayed similar trend, as HT appeared to decrease the fraction of cells in S-phase compared to samples treated at 37ºC. We postulated that

it could be due to a transitory cell cycle arrest caused by HT, which prevented initiation of S-phase for cells and possible fixation of crosslink damage.

The OVCA433 cell line had equal rates of apoptosis after treatment at 42ºC and 37ºC (fig. 16C/D), which upheld the thermo-tolerant behavior observed from viability assays. In contrast to the cell lines B76 and pmOC8, OVCA433 had higher fraction of cells in S-phase after treatment at 42ºC compared to 37ºC. The rate of apoptosis found 24 hours after cisplatin treatment at 37ºC were 29%, compared to 22% after treatment at 42ºC. OVCA433 appeared to be sensitive to mitomycin, as 63% cells were apoptotic after mitomycin treatment at 37ºC. Surprisingly, this fraction was lower (39%) in samples treated with mitomycin and HT. While the results from treatment at 37ºC were in compliance with the low viability observed after 72 hours by MTS assay, the lower fraction of apoptotic cells observed after combination treatment with HT could not be explained without additional time-points of analysis.

4.5.2 Cell cycle distribution after cisplatin treatment

The cell line responses detected by Hoechst and TUNEL assay after treatments were surprising. In most cases, drug treatments in combination with HT did not cause increased rates of apoptosis after 24 hours compared to treatments at 37ºC. In contrast to viability assays, where sensitizing effects of HT were observed with cisplatin for both B76 and pmOC8, only B76 showed small increase in apoptosis after HT combination treatment (fig. 16A). To determine if this could be due to specific interactions between HT and cell cycle progression, DNA histograms are shown (fig. 17).

The histogram for B76 showed a similar phenomenon as in pmOC8 (fig. 16A/B). A double-peak at the G1/S transition indicated that cells had attempted to start S-phase but shortly after stalled. It is likely caused by cells encountering cisplatin-induced crosslinks in DNA, making them unable to continue replication until the crosslink is resolved. As this effect is not seen for cisplatin in combination with HT, it is possible that HT induces a transitory G1-arrest in B76 and pmOC8 that

prevented S-phase initiation until after 24 hours. However, this hypothesis could only be confirmed by examination of cell cycle distribution at several more time-points after treatment. In contrast, the cell cycle distribution of OVCA433 did not appear to be affected by HT (fig. 17D).

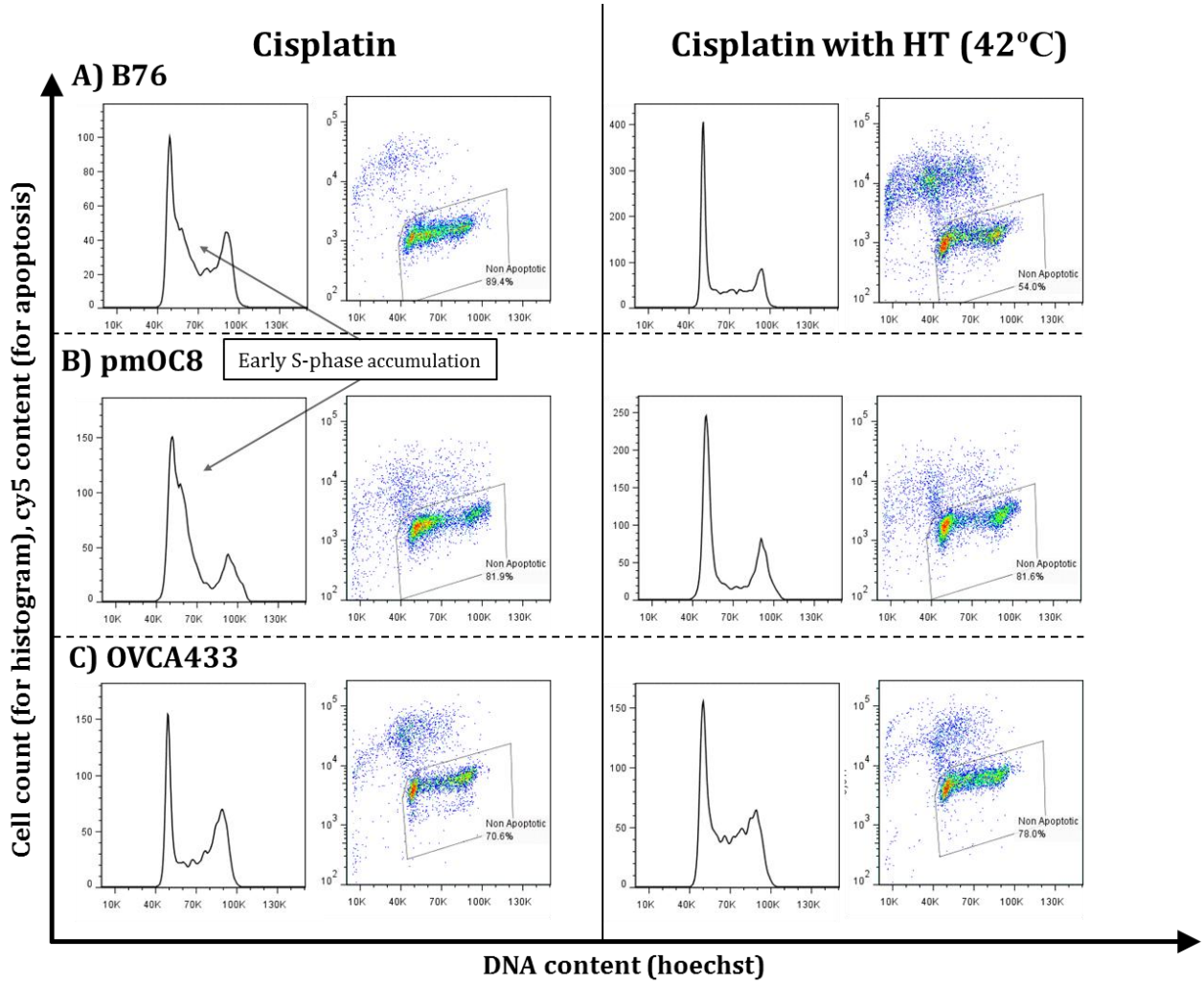

Figure 17: Histograms of DNA and apoptosis measurements from TUNEL assay 24 hours after cell treatment. Figure shows the distribution of cell lines after treatment with cisplatin with or without HT (42°C). Note the sharp peak immediately following G1-phase for **A)** B76 and **B)** pmOC8 treated with cisplatin at 37°C. Both cell lines have likely attempted to initiate S-phase but have encountered cisplatin crosslinks, stalling replication. **C)** OVCA433, on the other hand, has high G2/M-arrest at 37°C and accumulation in S-phase at 42°C. Note the increase in apoptosis of **A)** B76 after treatment with both cisplatin and HT.

4.5.3 Cell cycle and apoptosis in B76 after 72 hours

To determine if the rate of apoptosis seen in B76 24 hours after HT (27%) was maintained at the duration used for viability assay, we investigated the cell cycle distribution and apoptosis in this cell line 72 hours after treatment. While cell cycle distribution appeared similar, apoptosis detected by TUNEL-assay was 3% and 14% in normal versus HT treated sample, respectively (figure 18). The fraction of apoptotic cells was 27% after 24 hours and 14% after 72 hours, suggesting the effects of HT on B76 apoptosis can be delayed over 72 hours. For a complete overview over data obtained during flow cytometry analysis, see appendix 5.

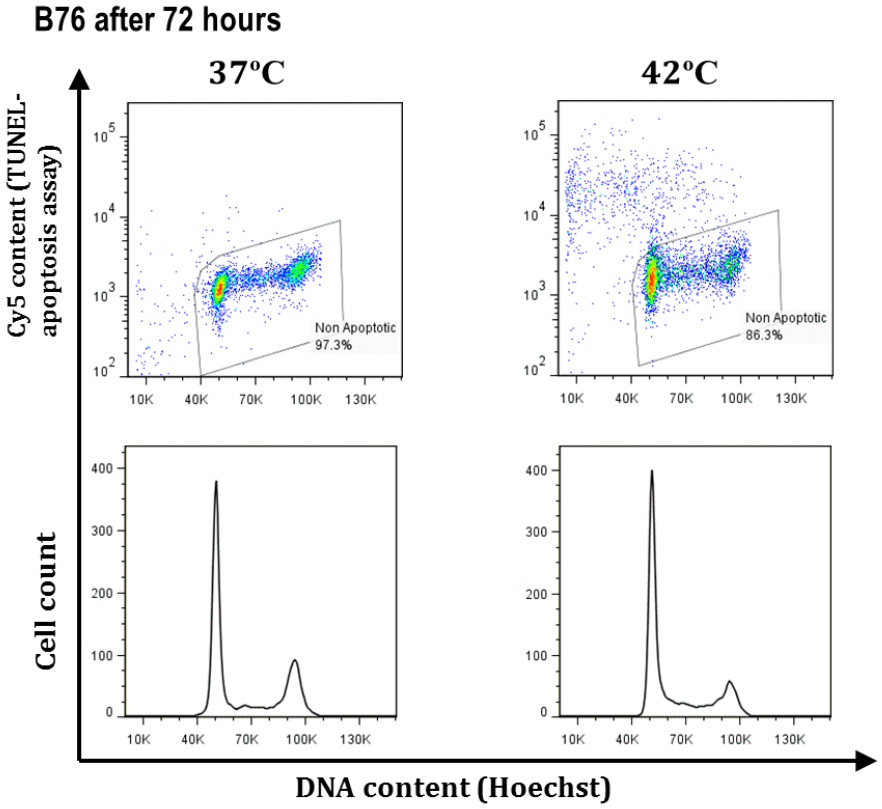

Figure 18: Histogram of DNA content as well as apoptosis stained with TUNEL. The B76 control samples (no drug) treated at 37°C and 42°C. Cells were analyzed after 72 hours recovery in incubator. The amount of apoptosis was detected by TUNEL staining (top), note 14% apoptotic cells from HT alone, which decreased from 27% as detected 48 hours earlier.

As the fraction of apoptotic B76 cells treated with carboplatin indicated that the cell line was responsive and not resistant as previously assumed, we analyzed samples

treated with carboplatin after 72 hours. To our surprise, the assumed carboplatin-resistant B76 did respond to carboplatin if treated in combination with HT. This sensitizing effect could not be detected by viability assays, where viability was observed to decrease only marginally (fig. 11).

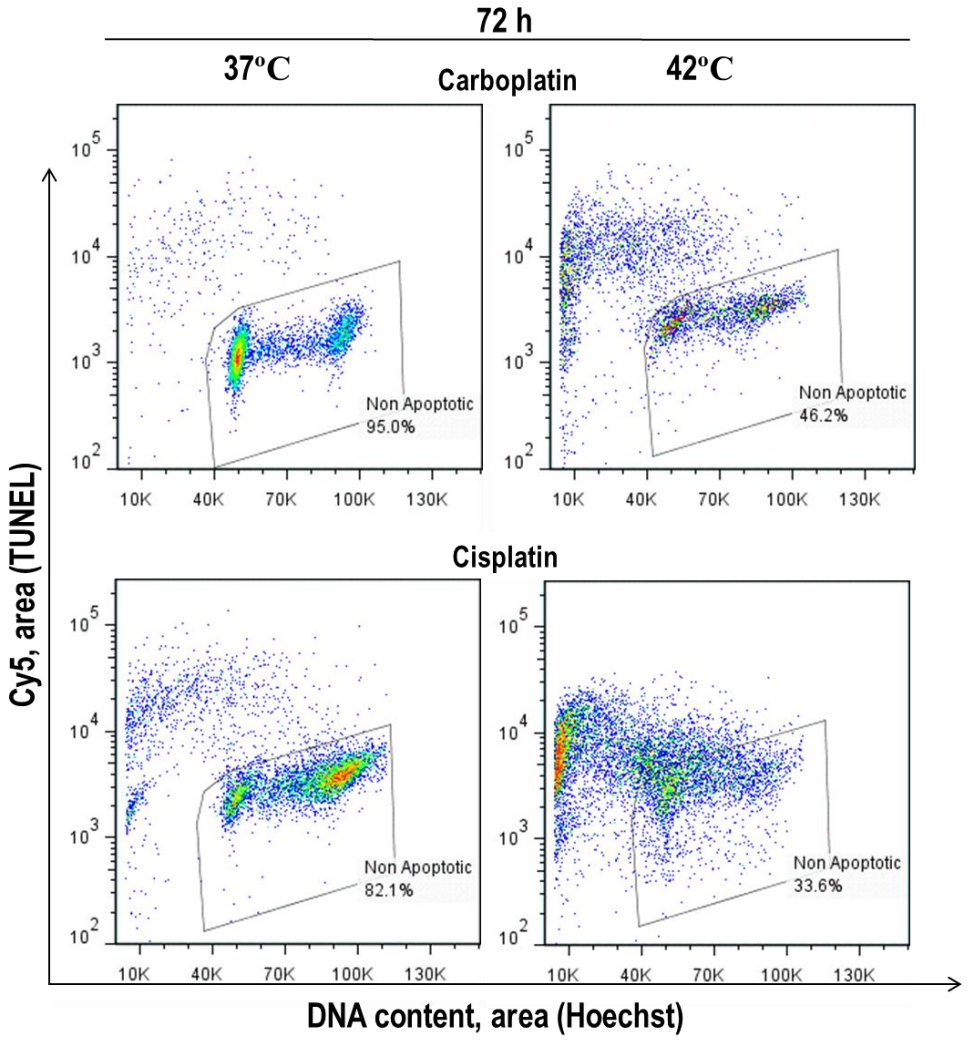

Figure 19: TUNEL assay 72 hours after treatment of B76 with carboplatin and cisplatin. Notice the high fraction of apoptotic cells after combination treatment at 42°C for both drugs. Accurate determination of the apoptotic fractions becomes impossible when there is no clear distinction between apoptotic and living cells, as observed in B76 sample treated with cisplatin and HT.

The cell lines pmOC8 and OVCA433 were not analyzed after 72 hours due to time constraints. Analysis of B76 after 72 hours, however, revealed higher apoptotic fractions resulting from combination treatment. Compared to the apoptotic fractions

observed after 24 hours, these observations suggest that drug treatment induces apoptosis faster in cells treated at 37ºC. Figures represent one biological replicate. As samples from B76 after 72 hours incubation contained high amounts of cell fragments (fig. 19), it must be made clear that accurate interpretation of data was difficult and only provided an estimation of the apoptotic fractions.

4.6 Protein expression analysis

Results from cell viability assays showed various cell line responses to cisplatin and mitomycin in combination with HT. In addition, results from TUNEL-staining indicated that viability measurements could not predict the cellular events that protrude them. Todetermine if cell response could be linked to HSP70 expression, we began by confirming antibody binding by western blot (data not included). After confirming bands of appropriate molecular weight, we proceeded with analyzing cell lysates extracted 24 hours after treatment using Peggy Sue technology.

4.6.1 Selecting normalization protein

Using house-keeping proteins to normalize signals detected during immunoassays is common. However, treatment with HT can disrupt protein expression, even expression of otherwise stably expressed house-keeping genes. We decided to investigate and compare the relative expression of b-actin and GAPDH after HT, to determine if either was suitable for normalization.

24 hours after the 90 minute treatment at 37ºC and 42ºC, pmOC8 lysates were prepared as previously described. The lysates were diluted to approximately 0.2 µg/µl and plated in duplicate to allow B-actin and GAPDH detection in identical samples. HT did not significantly affect b-actin expression 24 hours after HT in pmOC8 (fig. 20A), however, signal from identical samples indicated reduced expression of GAPDH after HT (fig. 20B). The detected GAPDH signal from HT treated sample was 30% lower (fig. 20C).

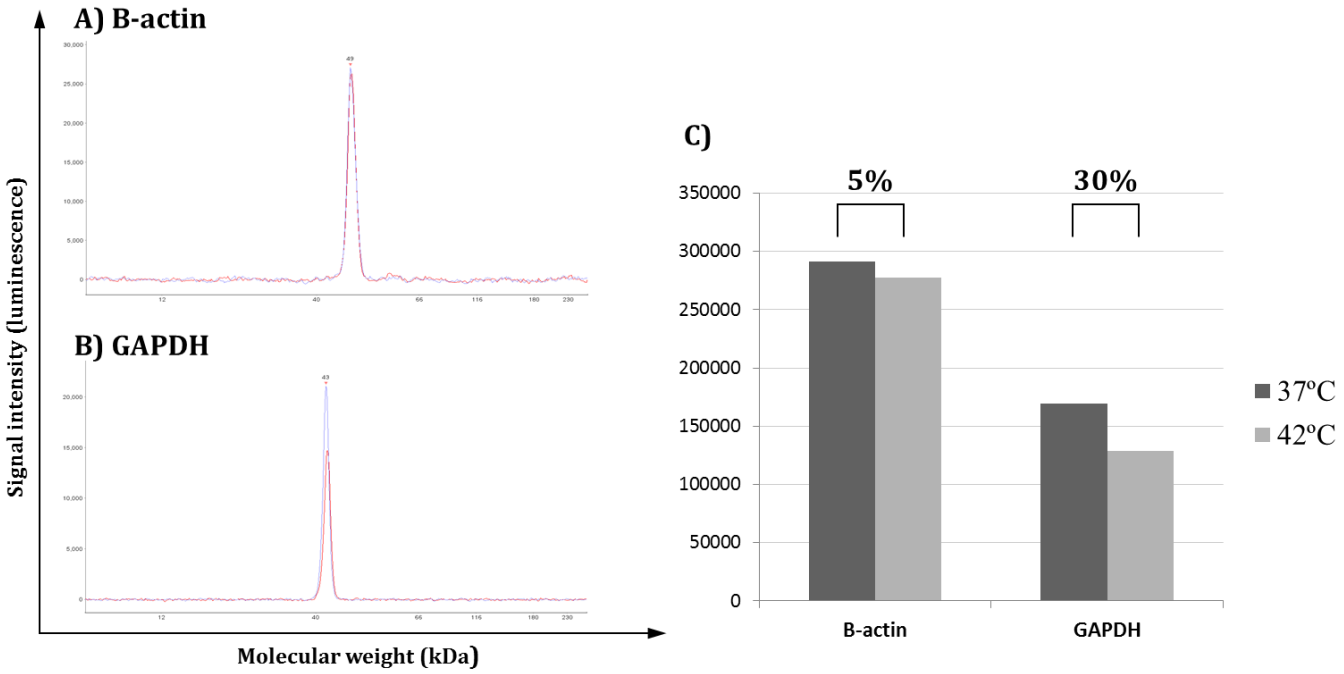

Figure 20: Results from expression analysis of the house-keeping proteins b-actin and GAPDH from pmOC8 after HT. **A)** Overlaid signals obtained from B-actin antibody, signal between samples show continuity. **B)** Overlaid signals for GAPDH antibody, notice how signal drops in sample treated with HT (37ºC = blue line, 42ºC = red line). **C)** Signal analysis revealed a 30% difference in the expression of GAPDH after HT compared to control (37ºC).

Because of the relatively large decrease in GAPDH expression observed by Peggy Sue analysis, we decided to use b-actin for normalization. Due to time constraints we did not analyze the expression differences in b-actin and GAPDH in other cell lines, although it would have been preferred. Instead, we assumed the expression of b-actin to be relatively stable after HT treatment in the other cell lines.

4.6.2 Optimizing signal detection of HSP70

To analyze HSP70 expression, we first attempted to use 0.8 µl/µg pmOC8 protein lysates and 1:150 dilution of the HSP70 antibody, but signal was saturated. We then reduced the pmOC8 lysates to 0.4 µl/µg and attempted with previous concentrations of HSP70 antibody (fig. 21). The signal was once again saturated (fig. 21A); however, the separation of the signal peak noticed in the HT treated sample (fig. 21B) indicated that HSP70 expression could be higher in this sample. The observed split

occurs when large amounts of bound HRP-conjugated antibody quickly deplete its substrate.

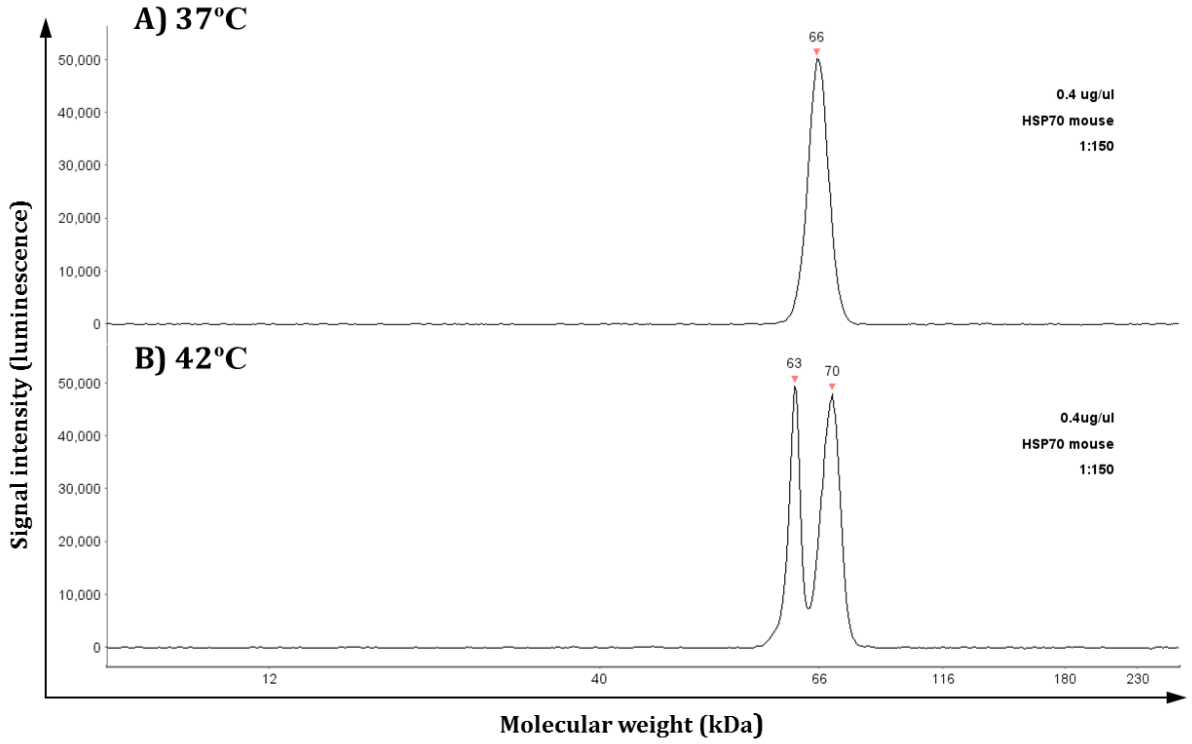

Figure 21: Signal from pmOC8 samples treated at **A)** 37°C and **B)** 42°C. Notice how the peak signal splits, an indicator of saturated signal.

Next, we attempted to lower the protein concentration of the pmOC8 samples to 0.1 µl/µg to obtain signals that could be used for further analysis. While the signal of the 37°C sample was acceptable (fig. 22A), the signal from 42°C was still near saturation level (fig. 22B). Unfortunately, the b-actin signal obtained at this lysate concentration was low and resulted in significant amounts of background noise (fig. 22C). It appeared that the signal intensity of HSP70 as a result of strong antibody binding, excessive HSP70 protein, or both, could not easily be coupled with b-actin normalization.

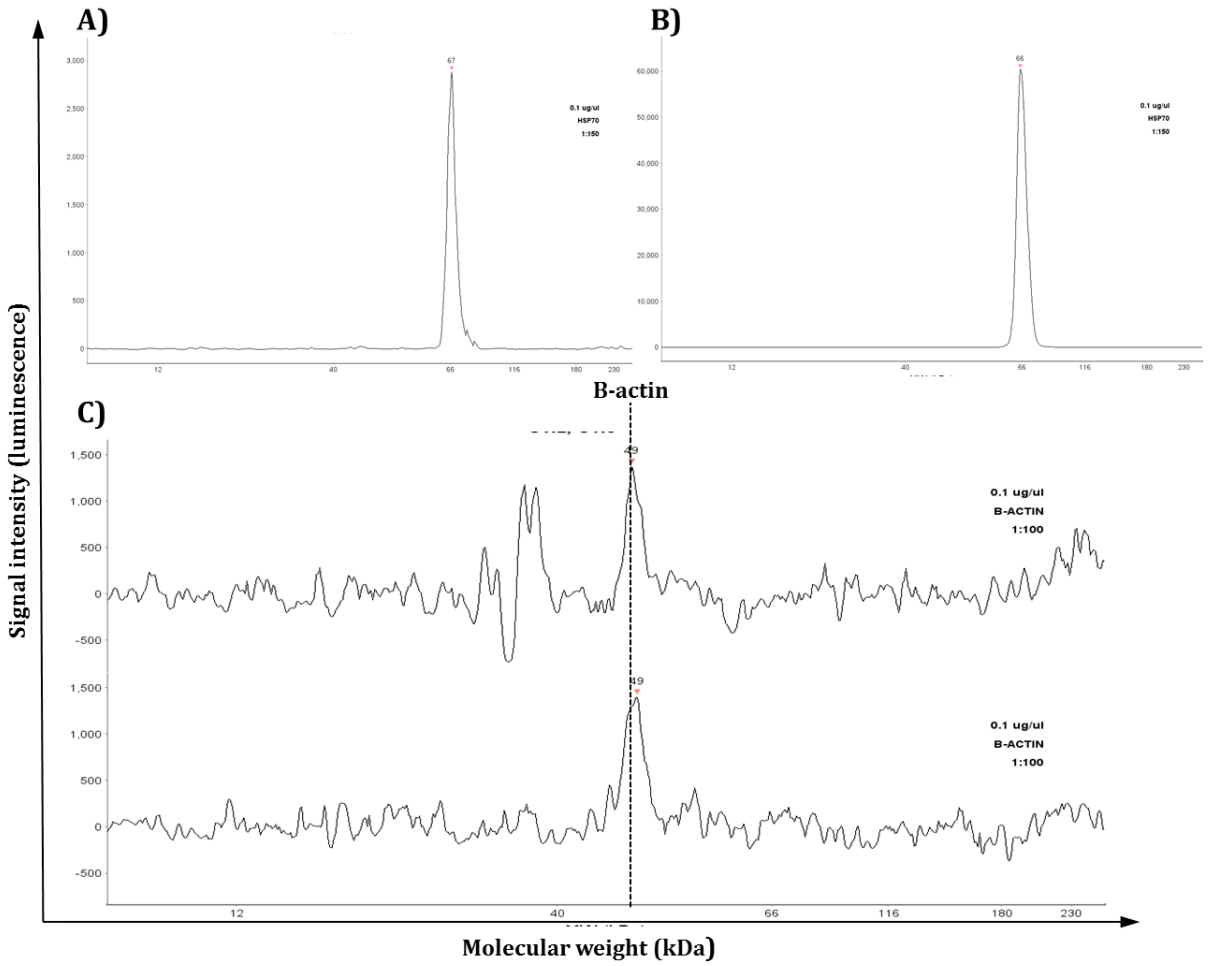

Figure 22: Results from optimization of HSP70 signal from pmOC8. **A)** Sample treated at 37ºC had appropriate HSP70 signal intensity and low noise. **B)** Sample treated at 42ºC had significantly higher HSP70 signal, and was likely saturated. **C)** B-actin signal was low and background noise was considerable at 0.1 µl/µg. For **C),** the top line corresponds to sample treated at 37ºC and bottom line to 42ºC.

To circumvent this issue we doubled the protein lysate concentrations to 0.2 µl/µg to optimize b-actin detection, and decreased HSP70 antibody concentration from 1:150 to 1:300 to reduce HSP70 signal intensity. While signal was not optimal, the HSP70 signal obtained could be used for estimating the relative expression increase of HSP70 within pmOC8, OVCA432 and CaOV3.

The HSP70 signal was high in both control and 42ºC for CaOV3, suggesting either an increased expression of HSP70 in this cell line from treatment procedure alone (including detachment by trypsin), or that CaOV3 had high basal expression of

HSP70 (data not shown). To enable comparison of cell lines with, most likely, different expression levels of b-actin, signal for HSP70 at 37ºC was set to 1 for control, and expression fold change was calculated within each individual cell line (fig. 23).

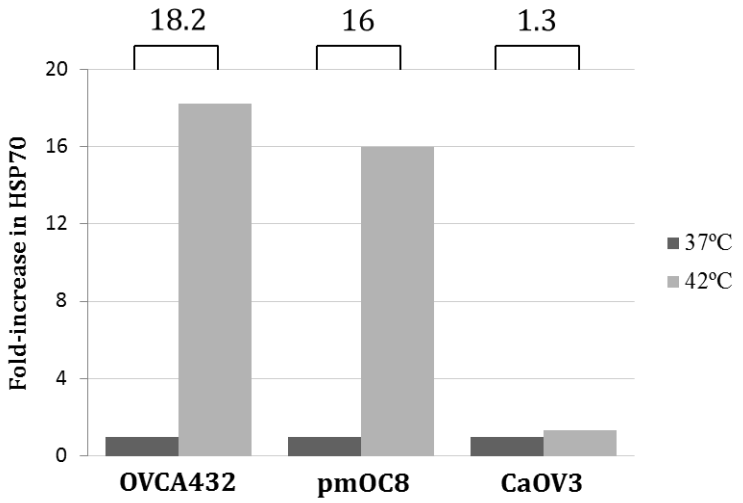

Figure 23: Estimated fold-increase in HSP70 expression in OVCA432, pmOC8 and CaOV3 after HT treatment. Figure is based on signal detected during Peggy Sue analysis.

The fold change in HSP70 expression between the HT and control sample was only 1.3 for CaOV3 (fig. 23). In contrast, HSP70 expression increased 16-fold and 18-fold in pmOC8 and OVCA432 after HT, respectively. We could not determine the expression levels of HSP70 accurately as signal was saturated, and refining the signal would require additional optimization. It is, however, interesting to note that the cell line CaOV3 appeared least resistant in viability assays from in vitro treatment, and had the lowest HT-induced HSP70 expression of the three cell lines analyzed.

Based on these results, we concluded that further optimization was required to accurately determine HSP70 expression in the other cell lines, including B76 and OVCA433. With high observed signal strength from incubation with the HSP70 antibody, accurate analysis of HSP70 expression would require us to either reduce lysate concentration, and determine protein concentration by other methods, or use new primary antibodies for HSP70 and B-actin. Alternatively, we could select

another house-keeping protein with higher basal-level expression. Regardless, determining the effects of HSP70 expression after in vitro treatment would also require analysis at several time-points after treatment. We attempted to analyze HSP90 expression in pmOC8 after HT, but no increase in expression was observed. While analysis of HSP27 revealed increased expression in pmOC8 after HT, the signal was saturated and optimization of HSP70 was prioritized instead. Data from Peggy Sue analysis of HSP27 and HSP90 are therefore not included.

4.7 Measuring the effect of MOC31PE by MTS viability assay

While results from cell viability and TUNEL assays confirmed that responses to treatment using the in vitro HIPEC model was cell line-specific, we turned to examine MOC31PE and its potential in HIPEC. MOC31PE is an immunotoxin consisting of a MOC-31 antibody, which binds the EpCAM surface antigen, conjugated to Pseudomonas exotoxin (PE). PE kills cells by inhibiting protein translation through ADP-ribosylation of the elongation factor 2 (EF-2) [89]. Compared to mitomycin, cisplatin and carboplatin, who all act mainly on DNA, MOC31PE presents a completely different mechanism for killing cancer cells.

4.7.1 All cell lines express EPCAM

To determine if the cell lines would be susceptible to MOC31PE, cells were stained with Ugelstad beads. All cell lines were EpCAM-positive by Ugelstad staining, and figure 24 shows B76 and OVCA433 positive staining (CaOV3, OVCA432 and pmOC8 not included).

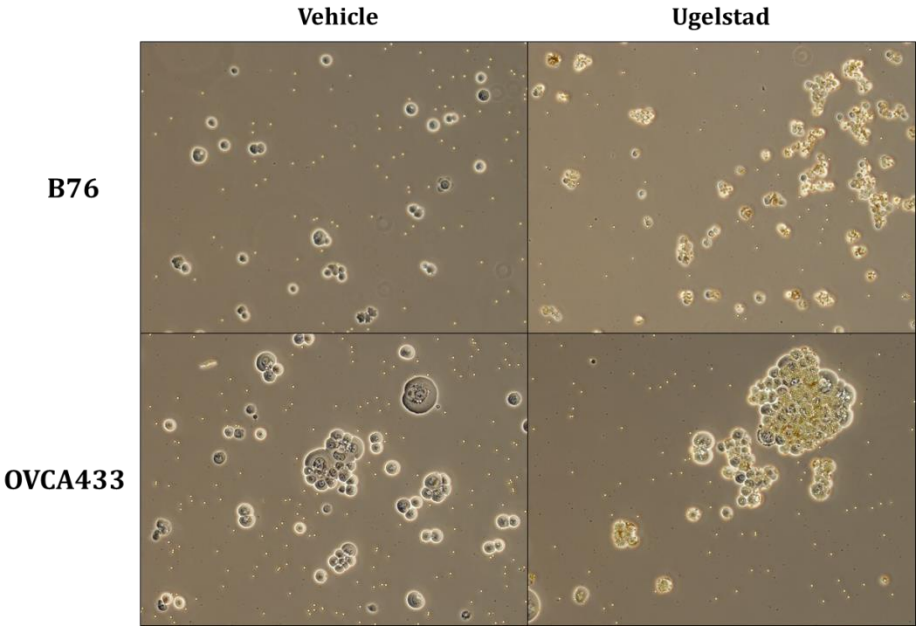

Figure 24: Both B76 and OVCA433 express EpCAM surface molecules and binds Ugelstad-beads. Note the aggregation of cells that form as Ugelstad bead is covered with many MOC31 antibodies, enabling binding of several cells at once. Picture is taken at 400X amplification.

4.7.2 Treatment of B76 and OVCA433 with MOC31PE

The results from viability assay after MOC31PE treatment revealed its cytotoxic effect on the cell lines B76 and OVCA433.

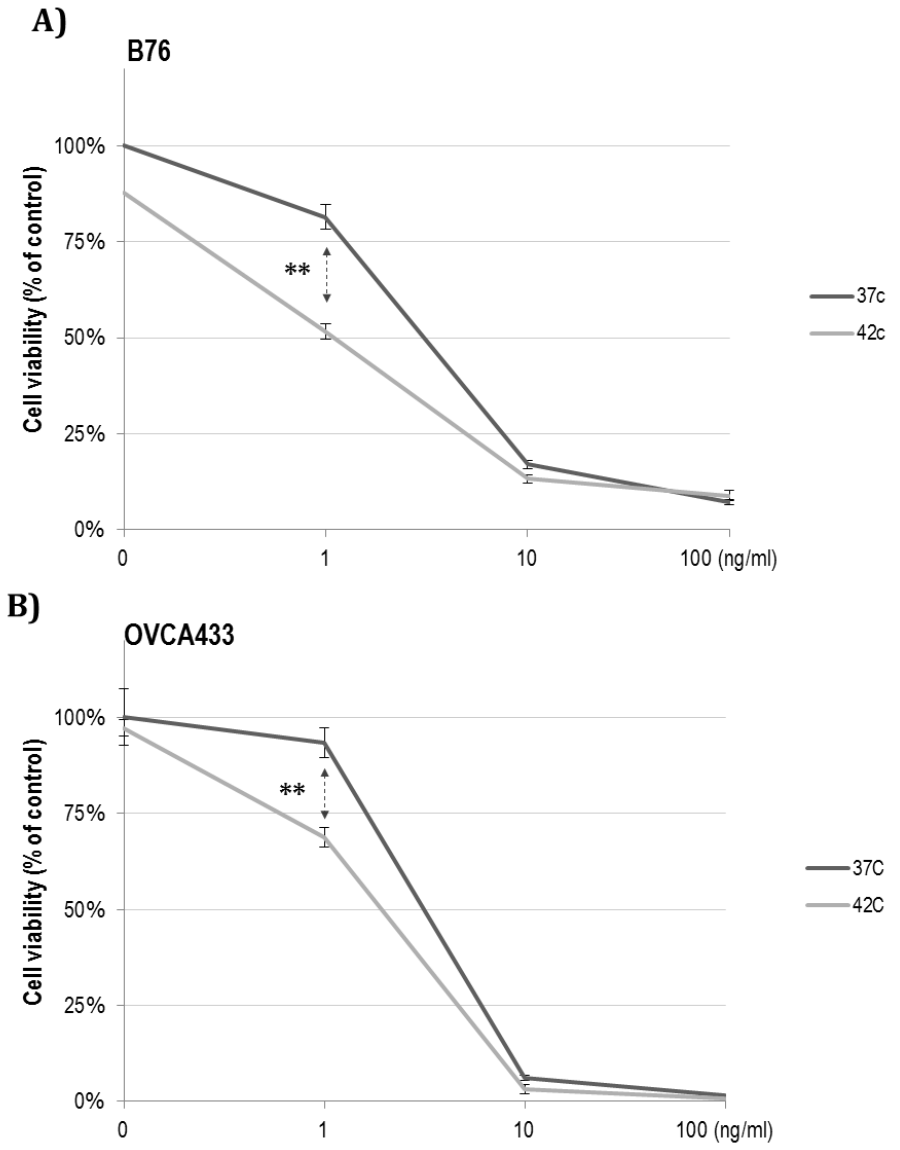

Figure 25: Viability of **A)** B76 and **B)** OVCA433 measured by MTS assay 72 hours after MOC31PE treatment. While B76 and OVCA433 appear dead at concentrations above 10 ng/ml, HT sensitized both cells lines to MOC31PE at the lowest concentration (1 ng/ml) and the differences were statistically significant. Note that only one biological replicate of the experiment was completed, and statistical analysis was completed on the triplicate dataset instead.

The effect of MOC31PE treatment at 1 ng/ml appeared to be potentiated by HT with both B76 and OVCA433 (fig. 25). These results stand in contrast the previously temperature-independent response of OVCA433. Only one biological replicate was complete for both cell lines, and statistical analysis was made on triplicate dataset from each replicate instead.

4.7.3 Cell lines are sensitive to MOC31PE

Before treating B76, OVCA433, OVCA432 and pmOC8 with MOC31PE, we decided the maximum concentration to be 10 ng/ml, as viability data from B76 and OVCA433 treatment demonstrated complete cytotoxicity above this concentration (fig. 26).

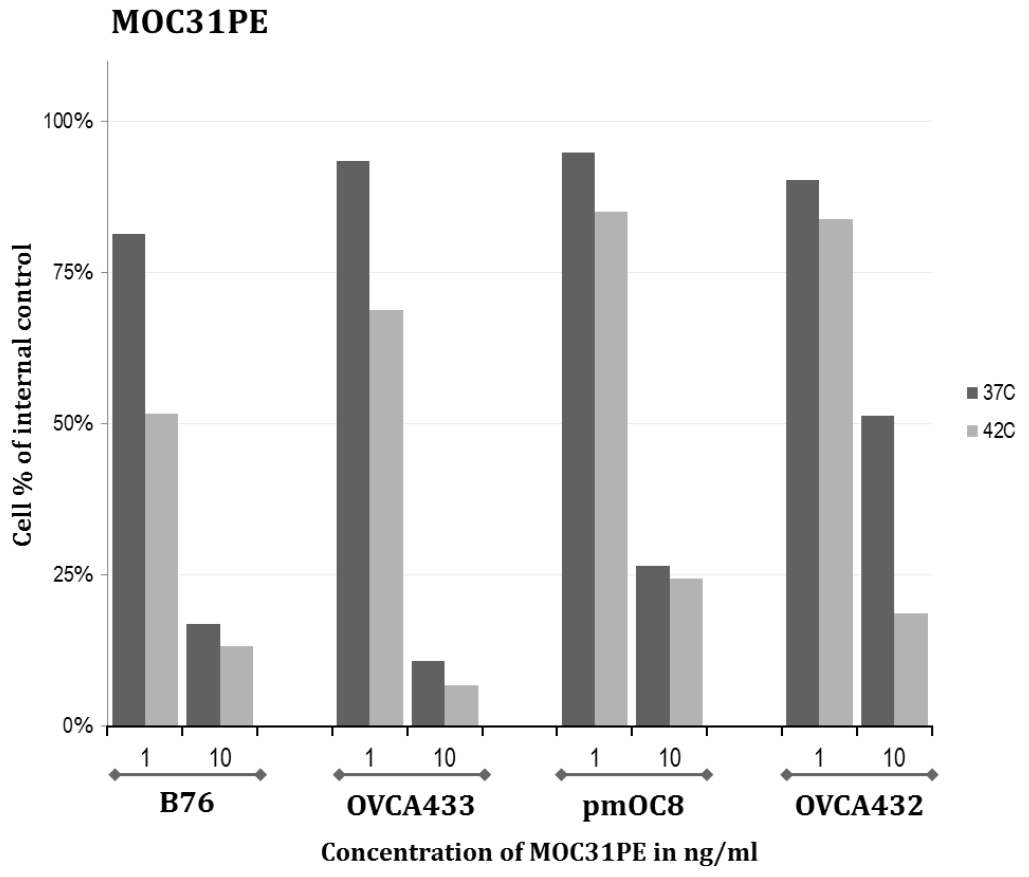

Figure 26: The effect of two concentrations of MOC31PE on cell lines B76, OVCA433, pmOC8a and OVCA432 at 37ºC and 42ºC. No statistical analysis was made. Note, however, the dose-dependent cytotoxic effect observed across all cell lines. Only OVCA432 appeared to maintain some viability after

treatment with 10ng/ml MOC31PE, however, HT appeared to further decrease its viability at this concentration.

All cell lines responded to MOC31PE, even at lowest concentration 1 ng/ml (fig. 26). HT appeared to increase the effect of MOC31PE in OVCA432, but statistical analysis was not completed.

5 Discussion

In the present work, we successfully established an in vitro model mimicking the conditions of HIPEC. Using this model, the response to HT was found to be cell line specific. While sensitizing effects of HT was observed in combination with chemotherapy agents, the extent of this effect varied greatly within cell lines as well as between the different drugs tested. Results indicate that while the clinical benefit of HT during HIPEC may depend on the patient-specific tumor profile.

5.1 Determining drug combinations for optimal cytotoxic effect in HIPEC is crucial for treatment outcome

The ultimate goal of cancer therapy is to remove or kill any cancer cell within the patient. For patients with metastatic OC, recurrence after primary treatment is often confined to the peritoneal cavity, suggesting that conventional methods struggle in eliminating residual disease. HIPEC has been developed to treat detached cancer cells and microscopic tumors left behind after surgery, but HIPEC efficacy depends on selected drug(s) and its potency in removing residual disease. As mentioned in a review by Beeharry et al. (2016), drugs used for HIPEC should have high cytotoxicity even at short exposure times, require no metabolic transformation, have pharmacokinetic advantages from IP administration and preferably show synergy with HT [90]. Pre-clinical studies investigating the effect of HT on drug treatments tend to use prolonged drug incubations or temperatures which are not obtained in the clinic. Here we presented an in vitro model that allowed assessment of cell line response to drug concentrations and exposure durations relevant to clinical HIPEC [44, 91, 92].

We found the most potent chemotherapy drug at the clinical concentration to be mitomycin, making it a clear candidate for HIPEC. However, a sensitizing effect of HT in combination with mitomycin was only observed in the B76 cell line. The cell lines OVCA433 and CaOV3 appeared more responsive to clinical mitomycin concentrations than other cell lines within the panel, which could suggest an alternate mode of action in these cell lines. While mitomycin, similar to carboplatin

and cisplatin, act mainly by crosslinking nuclear DNA, it can also target mitochondria and disrupt mitochondrial membrane potential [93-95]. OVCA433 has been shown previously to be sensitive to the mitochondria inhibitor Rotenone, due to high dependence on mitochondrial respiration [96], and it is possible that the underlying mechanism is mitochondrial malfunction in both cell lines. Further investigation of mitochondria involvement in OVCA433 and CaOV3 response to mitomycin is required to determine the mechanisms involved.

5.2 Cells are sensitized to cisplatin by hyperthermia

In contrast to mitomycin, HT sensitized the cell lines B76, CaOV3 and pmOC8 to cisplatin. The sensitizing effect of HT on cisplatin has been observed earlier [97-99], but is rarely investigated simultaneously in several cell lines as we have done in this study. The underlying mechanisms of cisplatin sensitization are still poorly understood. When samples were 24 hours after cisplatin treatment by flow cytometry, the rate of apoptosis was, paradoxically, higher in cells treated at 37ºC compared to 42ºC. A high fraction of cells in both pmOC8 and B76 appeared 'stuck' in early S-phase (fig. 17). One hypothesis, briefly mentioned in the result section, is that cells treated at 37ºC progressed faster from G1-phase into S-phase compared to cells treated with HT, where replication machinery would encounter cisplatin crosslinks and stall. As this early accumulation in S-phase is not seen in cells treated at 42ºC (fig. 17), it is possible that HT induces a temporary G1-arrest and blocks G1/S transition, or that G1-arrest is result of accumulated DNA damage that may come as a direct result of HT. Regardless, the actual fixation of cisplatin-induced crosslinks into single-strand or double-strand breaks would likely increase as cells attempted to enter S-phase. By analyzing B76 cells 72 hours after treatment with cisplatin, we found rate of apoptosis to be 20% in control compared to nearly 70% in the HT-treated cells (fig. 18). Unfortunately, we did not analyze OVCA433 or pmOC8 on flow cytometry 72 hours after treatment. However, results indicate that while HT sensitizes cells to cisplatin-induced damage, the final stages of apoptosis appear to be delayed by HT compared to treatment at 37ºC.

HT can sensitize cells to DNA damage by affecting the affinity of proteins that interact with DNA. Van der Waal et. al. found HT to induce enhanced binding of DNA-binding proteins, and that S-phase delay could reduce HT cytotoxicity in S-phase cells [100]. As OVCA433 appeared thermo-resistant in both viability and apoptosis assessment, it is possible that OVCA433, with wild-type TP53, has a more efficient and prolonged cell-cycle arrest compared to TP53-mutated B76 and pmOC8.

While the B76 cell line appeared unresponsive to carboplatin by viability assessment, analysis by TUNEL-assay revealed large fraction of apoptotic cells after treatment in combination with HT. As carboplatin is an analogue to cisplatin, it is not unlikely that similar mechanisms of HT sensitization to cells occur with carboplatin as cisplatin. HT can also sensitize cancer cells by increasing drug accumulation inside the cancer cell, which has been shown for carboplatin previously [101]. The observed effect of HT could therefore be a combination of both drug accumulation and modulation of the DNA repair machinery. Further studies are needed to confirm the role of HT on DNA-repair, carboplatin and cisplatin sensitization, especially in the time-frames relevant for HIPEC. The results serve as a reminder that flow cytometry only provides a snapshot into cellular 'conditions', and cellular events go unnoticed if cell response is analyzed by using viability assays alone. Confirming the role of HT regarding cell cycle progression and the sensitization effect will require additional time-points of analysis. Regardless, the results show that cisplatin in combination with HT have synergistic tendencies which are beneficial for HIPEC, but that the effect will depend on cancer-specific characteristics, including TP53-status [102]. Further studies on HT-drug interactions aimed to improve HIPEC efficacy should incorporate drugs with different modes of action, such as taxanes, to determine if the main sensitization effect of HT is through DNA damage or other mechanisms.

5.3 A potential role of cell detachment in OVCA433 treatment response

The largest differences in response to HT were between the cell lines B76 and OVCA433. While B76 was highly sensitized to cisplatin and mitomycin in combination with HT, no response to HT was seen with OVCA433. OVCA433 also had equal amount of apoptosis after treatment with HT compared to control (fig. 16D). It is possible that the treatment procedure itself, including detachment from the culture flask by trypsinization, was capable of inducing apoptosis in the OVCA433 cell line. Cells are often dependent on cell-to-cell and cell-extracellular-matrix binding for proliferation and, although most malignant cells possess altered contact dependence, cancer cells which are anchored to ECM or grown as 3D-speroids are generally more resistant to treatment in vitro [103, 104]. Indeed, cleavage of membrane proteins by trypsinization has been shown to induce expression changes in apoptosis-related proteins [105]. However, as only a single flow cytometry analysis of OVCA433 was made, it is possible that the effect was a result of extended incubation with trypsin prior to treatment, as pmOC8 and B76 appeared unaffected by the treatment procedure itself (control 37°C). Man-made errors in treatment protocol are unavoidable but can be accounted for by repeating the observation in several biological replicates, which means additional experiments are required to confirm the role of detachment for OVCA433 apoptosis. Further investigation could also include methodical adaptions that allow cells to be treated while still anchored in monolayer, or through implementation 3D-cell culturing to maintain cell-to-cell contact. 3D-cell cultures could be used with the herein established model to allow investigation of HT effect on drug penetration into tumor nodules, an important factor for HIPEC outcome.

Viability assays have limited information value, and must be supplemented with other methods of analysis to draw conclusions on the effect of drug treatment. Apoptosis caused by the treatment in OVCA433, for instance, could not be detected by viability assays alone. However, the model provided consistent viability readings within experiments on the same cell lines.

5.4 HSP70 expression is induced by HT in cell line OVCA432 and pmOC8

Cancerous cells tend to have modulated HSP expression and high expression of HSPs have been linked to treatment resistance [106]. Interestingly, we found the expression of HSP70 in CaOV3 to be constitutively high, much higher than in cell lines OVCA432 and pmOC8 at 37ºC. However, the expression of HSP70 increased only 1.3-fold after HT, compared to 18- and 16-fold in OVCA432 and pmOC8, respectively. CaOV3 was the most sensitive cell line to combination treatments with HT. As such, the capacity to induce HSP70 expression might be more important for its cytoprotective and anti-apoptotic function during chemotherapy than the constitutive expression levels of HSP70 at normal conditions. However, for assessing the relationship between HSP70 and treatment response, analysis of HSP70 expression in cell lines treated in combination with mitomycin and cisplatin is required. Meanwhile, clinical trials on HSP-inhibitors are ongoing and hold promise as drug combination strategies for HIPEC.

Further optimization is required to refine the HSP70 signal detected by Peggy Sue. No conclusion is therefore made on the quantitative expression of HSP70 in the cell lines, as signal was approaching saturation when calculations were made. Due to time constraints, we did not investigate the expression increase of HSP70 in cell lines B76 and OVCA433. Determining the expression levels of HSP70 in these cell lines could elucidate whether the thermo-tolerant behavior shown by OVCA433 is due to HSP70 expression. Expression of HSPs has been shown to be induced after HT in a time-dependent manner [107], and accurate assessment of the HSP70's role in treatment resistance would require several time-points of analysis. It should be mentioned that Peggy Sue was a highly convenient instrument for protein analysis, but there are no shortcuts in quantitative expression analysis.

5.5 MOC31PE displayed cytotoxicity in all cell lines and was sensitized by HT

We observed a cytotoxic effect of immunotoxin MOC31PE on all cell lines within the panel (fig. 22/23, data for CaOV3 not included). Viability assays showed that MOC31PE effectively reduced viability at low concentrations regardless of HT. An interesting observation was the sensitizing effect of HT in OVCA433, which had been unresponsive to HT during cisplatin and mitomycin treatments. The same sensitization was seen with OVCA432, which appeared resistant to clinical concentrations of mitomycin and cisplatin. Although further biological replicates are required to draw statistical conclusions, a synergistic effect between MOC31PE and HT seem possible.

The pathways of DNA repair and HSPs expression, recurrent themes when discussing HIPEC efficacy, are dependent on protein translation. By inhibiting protein translation through MOC31PE, heat-stressed cells would be unable to activate selective translation of HSPs through the HSR and UPR-systems. Studies have also shown that HSPs are involved in stability of DNA repair proteins and could indirectly affect the DNA repair machinery within the cell [108]. Loss of HSPs expression within the cell could tip the balance in favor of apoptosis, which would explain the increased efficacy of MOC31PE in combination with HT. While analysis of MOC31PE cytotoxicity by flow cytometry is warranted, these results suggest a potential candidate role of MOC31PE in HIPEC drug combination strategies.

5.6 Cell culturing and in vitro research suffer from lack of heterogeneity

While cell line models remain efficient and dependable systems for drug screening, one should always be careful when translating in vitro observations to in vivo conclusions. The artificial culture environment continuously shapes the cell population, and studies have shown that much of the in vivo heterogeneity is lost during the cultivation process. Deleterious BRCA1/2 mutations, for instance, are found in 10-15% of serous OC [109-111], but are excessively rare in EOC cell lines

thought to represent the disease [80]. As a result, in vitro studies can indicate drug responses unlikely to translate to the clinic.

While culturing of cancer cells inevitably confer both morphologic and genotypic changes to the cell population resulting from a complete loss of tumor microenvironment, many molecular mechanisms of drug and treatment resistance are likely still in play. Drug resistance observed in the clinic is likely a result of cancer cell heterogeneity within tumor(s) of each patient, and predicting response to treatment based on cell line models is difficult [112, 113]. For in vitro studies to capture this heterogeneity, one must assume that each cell line represent a homogenous population of cancer cells and include several cell lines when investigating drug efficacy. An in vitro study which includes several cell lines will have stronger evidence that the observed response may translate to the clinic, which is why several cell lines were included in this study.

5.7 Viability assays provide limited information on cell response to treatment

There are methodical limitations to viability assays that must be addressed. Cell response to treatment was analyzed with MTS- and ATP assays and reported as % viability of the control. Viability measured by ATP assay was found to correlate almost perfectly with MTS data (appendix 4), which was not surprising considering both assays measure some form of metabolic activity. The assays could not determine the "true" viability within each sample, but rather estimate the growth inhibitory effect of each drug treatment compared to control. It was therefore unclear if the observed responses were either cytotoxic or cytostatic to the cells until cells were analyzed by TUNEL assay.

Several articles have been published on the subject of MTS viability and the accuracy of this method in determining cytotoxic response [114, 115]. Eastman (2016) criticized the widespread use of viability assays to determine drug efficacy, and suggested the use of two time-points of analysis to determine the relative growth within each sample [116]. When we analyzed the signals obtained from MTS

assays by subtracting signal at 72 hours with the signal obtained after 24 hours, we found the response curves of B76 and OVCA433 to be similar to data observed at the 72 hour time-point alone (appendix 3). There was, however, a clear discrepancy in the response compared to single time-point analysis at 72 hours. For B76, an increase in signal intensity relative to control was seen after treatment with both mitomycin and cisplatin at 37°C, indicating the survival and proliferation of cells after treatment. Only when combined with HT did the drug treatments result in a lower signal at the 72 hour time-point compared to the 24 hour time-point. While these results support the sensitizing effects of hyperthermia in B76, it also reinforces the notion that viability data must be carefully assessed, as well as supplemented by other methods of analysis. The time-points used to assess cell viability, as well as interpretation of the data, should be optimized to detect the actual cell response. Regardless, the established in vitro model provides a solid framework for analyzing the effect of combination treatment on cell lines in a HIPEC setting.

6 Final conclusions

Ovarian cancer remains a significant health burden. While promising targeted therapies lie on the horizon, conventional chemotherapy remain the foundation of OC treatment. HIPEC has shown survival benefit, but few pre-clinical studies have studied the interaction between HT and chemotherapy in a clinical HIPEC setting. Using an in vitro model, we present evidence that HT can sensitize cancer cell lines to chemotherapy during HIPEC, and that the response is both cell line specific and depend on the drug used. Few studies have investigated several drugs using many cell lines as presented here, and by doing so we obtained results which more accurately reflect the heterogeneity of OC. Further studies are required to uncover the molecular mechanisms responsible for the effect observed with each individual drug. Studies should aim to investigate gene variants present in cell lines that appear resistant, including OVCA432 and the HT-resistant OVCA433. Future adaptations include 3D cell culturing, co-culturing different cell-types including fibroblasts or macrophages, and including ex-vivo patient samples. These adaptations could easily be implemented with the model, and could provide cell heterogeneity required to bridge in vitro studies to clinical response. Lastly, the presented PM in vivo mouse model would be a natural candidate for further studies on drug interactions in HIPEC, the toxicity of combination treatments as well as efficacy in an in vivo setting.

Appendix 1: Reagents and buffers

Method&Buffer	Reagents	Cat. #
1X Running buffer		
50mL MES 0.95 L ddH2O	MES SDS running buffer (20X), Invitrogen	NP0002-02
10X Transfer buffer		
30.3g 144g 1 L	Tris (Merck, Millipore) Glycine (99.7%, VWR Chemicals) ddH2O	108382 1.04201.1000
1X Transfer buffer		
200 mL 100 mL 700 mL	Methanol (99.8%, VWR Chemicals) 10X Transfer buffer ddH2O	20847.307
Blocking buffer (TBS-T)		
5mL Tween20 (25% solution, in ddH20) 30 mL 5M NaCl 25 mL 1M Tris-HCl 940 mL ddH2O	Tween™ 20 (Fisher BioReagents™) NaCl (Sigma Aldrich) 1M Tris-HCl pH 7.5 (Thermo Fisher)	BP 337-500 433209 15567-027
Secondary antibodies		
Anti-rabbit Anti-mouse	Goat anti-rabbit, HRP-conjugated (Dako) Rabbit anti-mouse, HRP-conjugated (Dako)	P0448, Lot: 20003813 P0260, Lot: 00065545
Lysis buffer 1.5X		
2.5 mL 1M Tris 33.5 mL ddH2O 1.5 mL 5M NaCl 30 ul NP-40	1M Tris-HCl pH 7.5 (Thermo Fisher) NaCl (Sigma) NP-40 (Abcam)	15567-027 433209 142227
10X PhosSTOP		
1 PhosStop tablet in 1 mL ddH2O	PhosSTOP™ (Sigma-Aldrich®)	04906837001

7X cOmplete		
1 cOmplete tablet in 1.5 mL ddH2O	cOmplete™, EDTA-free Protease Inhibitor Cocktail (Sigma-Aldrich®)	04693132001
Lysis buffer (1X)		
755 uL 100 ul 145 ul	1.5X lysis buffer pSTOP (10X) cOmplete (7X)	
Flow cytometry		
Hoechst staining 1:400, PBS	Hoechst 33258 pentahydrate bis-benzimid (10mg/ml, Invitrogen)	H3569

TUNEL assay reagents (per sample)		
0.16 uL	TdT Enzyme	03333574001
4.0 uL	TdT 5X reaction buffer	16314015
2.4 uL	$CoCl_2$	11243306001
0.4 uL	Biotin-16-dUTP	11093070910
0.4 uL	DTT (dissolved in H2O to 10mM)	D0632-5G
32.64 uL	ddH2O	
Streptavidin-Cy5	Cy5-Streptavidin (GE Healthcare)	PA45001
Peggy Sue		
Master Kit 384-well plate	Peggy Sue or Sally Sue-Rabbit (12-230 kDa) Size Separation Master Kit Hard-Shell 384-well PCR Plate (BioRad)	PS-MK06 HSP3831
Reagents for 12-230 kDA Peggy Size (Purchased from ProteinSimple)	Stacking Matrix 2 Separation Matrix 2 Sample Buffer 2 Total Protein SA-HRP Antibody Dilutent 2 Anti-Mouse Secondary Antibody	042-513 042-512 042-195 042-976 042-514 042-205

	Upper Running Buffer	043-163
	Lower Running Buffer	043-164
	Luminol-S	042-521
	Peroxide	042-522
	Standard Pack 1	77032
	Anti-Rabbit Secondary Antibody	042-206

Appendix 2: Antibodies used for Western blot and Peggy Sue analysis

Antibody	**Cat #**	Western Blot concentration	Peggy Sue concentration
HSP27 (Cell Signaling)	95357S	1:1000	1:150-1:300
HSP70 (Cell Signaling)	46477S	1:1000	1:150-1:300
HSP90 (Cell Signaling)	4875S	1:1000	1:50
B-actin (Sigma)	A5316	1:2000	1:100
GAPDH (Sigma)	G8795	1:1000	1:150

Appendix 3: Using 72h/24h MTS data to estimate relative proliferation of cell lines

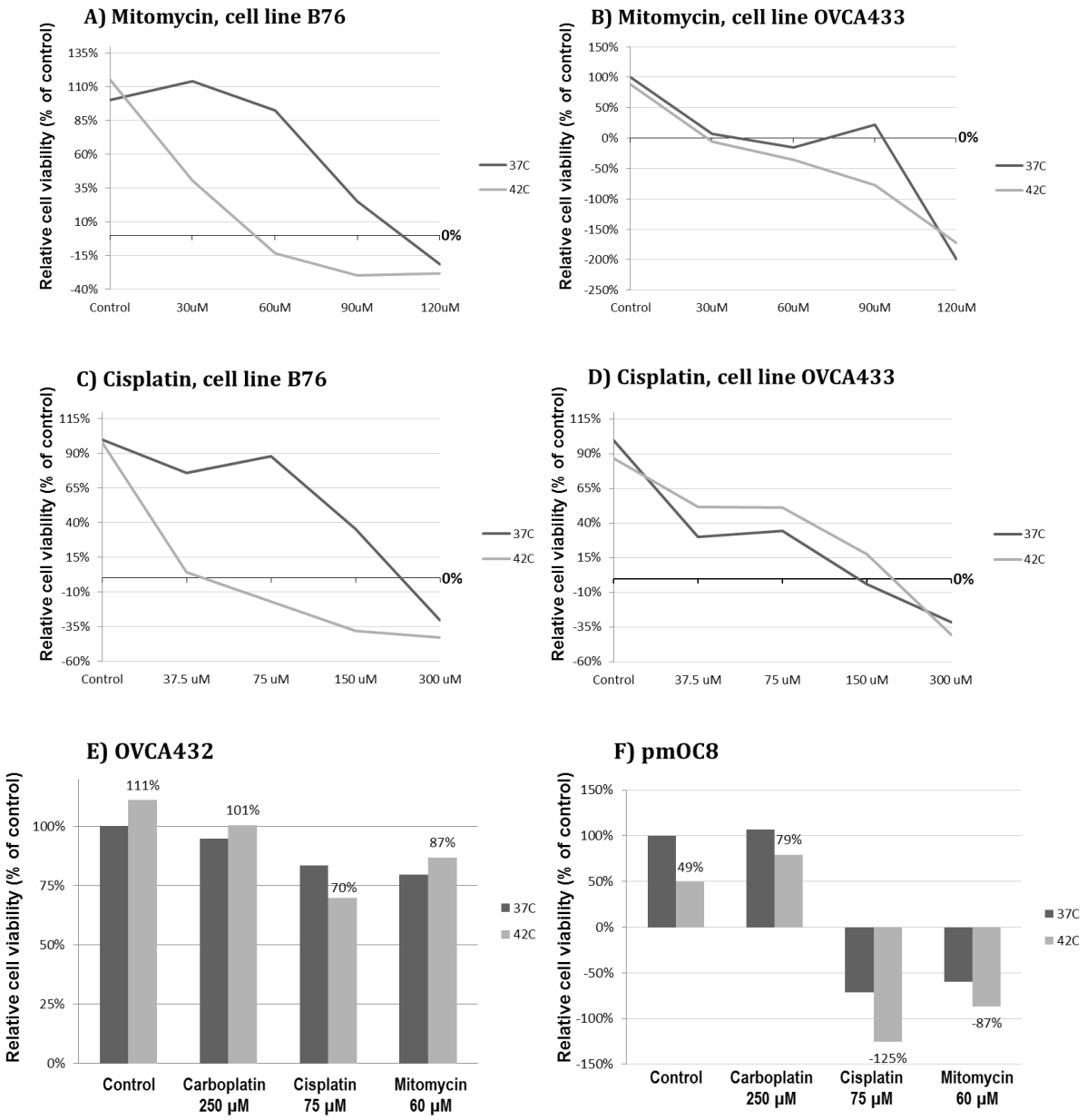

Appendix 3: Figures show the relative proliferation increase measured as 72 hour signal subtracted by 24 hour signal. **A)** Relative viability increase after treatment of B76 with mitomycin. Note the difference at the two temperatures. **B)** OVCA433 treated with mitomycin. **C)** B76 treated with cisplatin, **D)** OVCA433 treated with cisplatin, **E)** screening of OVCA432 and **F)** screening of pmOC8. Note how **E)** OVCA432 appear to grow after treatment with all drugs tested, while the signal from **F)** pmOC8 is decreased by cisplatin and mitomycin treatment. This 'alternative method' of analyzing MTS data can provide insights to the specific growth response within each sample.

Appendix 4: Comparison of MTS- and ATP assay in one single biological replicate

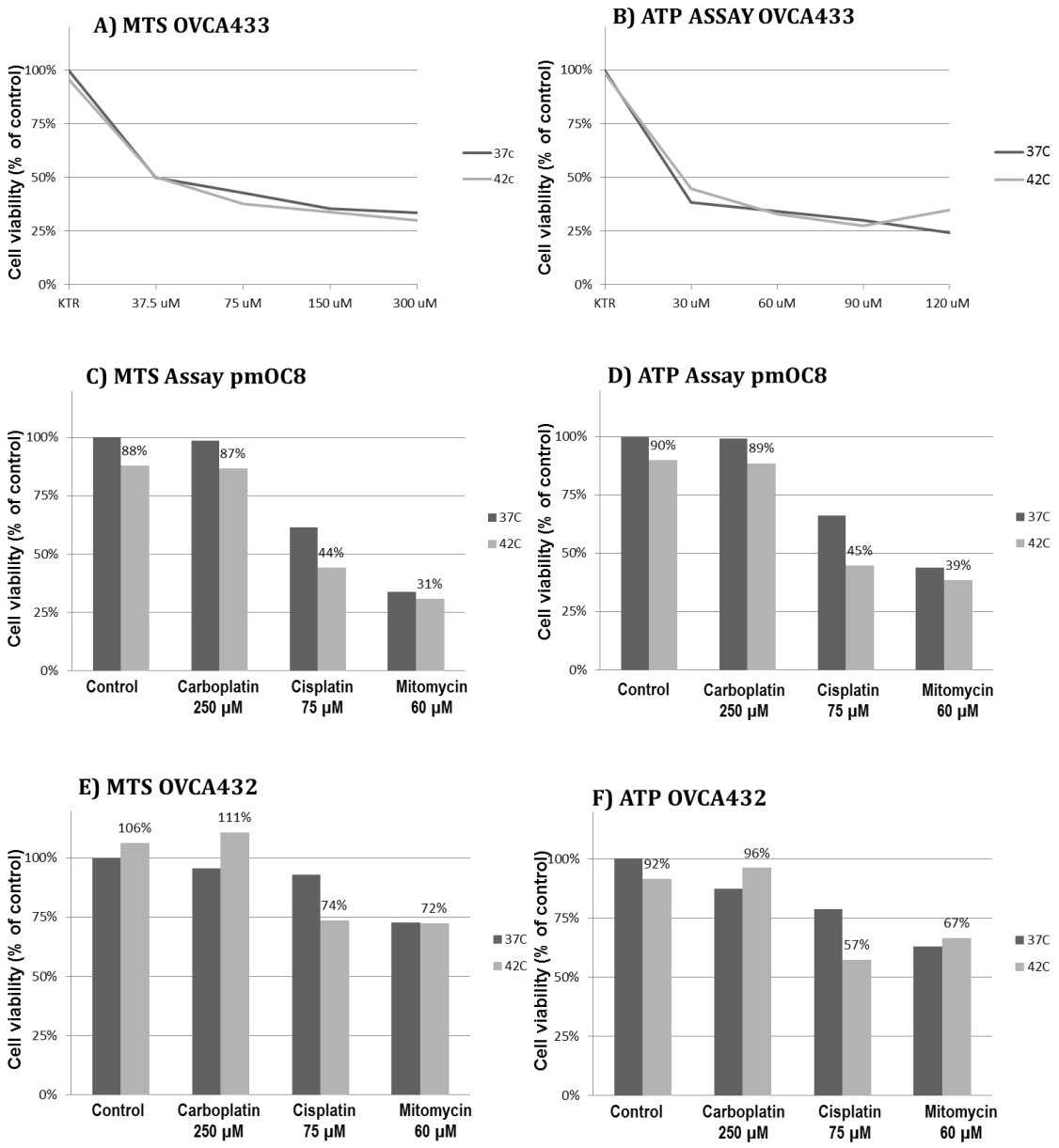

Appendix 4: Figure shows data from MTS and ATP assays preformed on identical replicate plates, confirming the high correlation between the two methods. **A)** OVCA433 MTS assay after *mitomycin* treatment correlates strongly with **B)** OVCA433 analyzed by ATP assay. Results from screening of pmOC8 and OVCA432 are also included. **C)** MTS assay of pmOC8 and **D)** ATP assay of pmOC8, and **E)** MTS of OVCA432 and **F)** ATP assay OVCA432.

Appendix 5: Flow cytometry data

Cell line		G1 - Phase	S - Phase	G2 - Phase	Apoptosis	Watson fit	Counted
B76							
	Prior to treatment (0h)	34%	57%	9%	2%	0.88	5358.5
	37ºC after 24h	25%	60%	14%	4%	0.545	3945.5
	42ºC after 24h	31%	51%	18%	27%	0.95	4941
	Cisplatin at 37ºC after 24h	16%	69%	15%	11%	0.66	4297
	Cisplatin at 42ºC after 24h	30%	56%	13%	37%	0.935	5464.5
	Mitomycin at 37ºC after 24h	24%	65%	11%	17%	1.145	5641.5
	Mitomycin at 42ºC after 24h	30%	57%	13%	28%	0.97	5150.5
	Carboplatin at 37ºC after 24h	17%	72%	10%	5%	0.5	4370
	Carboplatin at 42ºC after 24h	30%	52%	18%	32%	1.095	5496
	MOC31PE at 37ºC after 24h	30%	56%	13%	5%	1.205	5265
	MOC31PE at 42ºC after 24h	19%	68%	14%	18%	0.97	4837.5
B76 - after 72 hours*							
	37ºC after 72h	52%	25%	23%	3%	1.01	5550
	42ºC after 72h	52%	34%	14%	14%	0.62	5295
	Cisplatin at 37ºC after 72h	15%	57%	28%	21%	1.09	4954
	Cisplatin at 42ºC after 72h	42%	48%	10%	49%	1.03	3621
	Mitomycin at 37ºC after 72h	14%	77%	9%	18%	1.15	5471
	Mitomycin at 42ºC after 72h	13%	79%	8%	66%	0.89	2933
	Carboplatin at 37ºC after 72h	65%	19%	16%	5%	1.01	5300
	Carboplatin at 42ºC after 72h	20%	66%	14%	54%	1.09	4726
	MOC31PE at 37ºC after 72h	68%	28%	4%	5%	0.84	5615
	MOC31PE at 42ºC after 72h	34%	50%	15%	28%	0.47	2078
OVCA433							
	Prior to treatment (0h)	32%	60%	8%	1%	1	7634.5
	37ºC after 24h	52%	34%	14%	13%	1.42	4548
	42ºC after 24h	28%	50%	23%	13%	1.07	5017
	Cisplatin at 37ºC after 24h	26%	63%	11%	29%	0.69	4153
	Cisplatin at 42ºC after 24h	20%	69%	11%	22%	0.76	5596
	Mitomycin at 37ºC after 24h	35%	57%	8%	63%	0.9	2373
	Mitomycin at 42ºC after 24h	24%	65%	12%	39%	0.93	4381
pmOC8							
	Prior to treatment (0h)	50%	26%	24%	3%	1.38	5550
	37ºC after 24h	43%	27%	30%	3%	0.92	5741
	42ºC after 24h	35%	36%	29%	13%	0.84	5531
	Cisplatin at 37ºC after 24h	28%	57%	14%	18%	1.17	5355
	Cisplatin at 42ºC after 24h	43%	36%	21%	18%	1.38	5478
	Mitomycin at 37ºC after 24h	34%	57%	9%	31%	1.56	5059
	Mitomycin at 42ºC after 24h	38%	43%	19%	26%	1.41	5075

Appendix 5: Table showing all results obtained from flow cytometry. Cell cycle was measured by Hoechst staining, and the cell cycle distribution was analyzed using the Watson algorithm in FlowJo. Model fit is indicated by the 'root mean square' (RMS)-value is here marked as "Watson fit". The estimated cycle distribution is considered relatively accurate if RMS value >1.5.Note that B76 cells analyzed 72 hours after treatment were severely fragmented, which limits the accuracy of the analysis (even if RMS-values are <1.5). The column marked "Counted" refers to the number of counted, single cells within the sample. Generally, higher numbers of counted cells increases analysis accuracy.

References

1. Ferlay, J., et al., *Cancer incidence and mortality worldwide: sources, methods and major patterns in GLOBOCAN 2012.* Int J Cancer, 2015. **136**(5): p. E359-86.
2. Tomasetti, C., L. Li, and B. Vogelstein, *Stem cell divisions, somatic mutations, cancer etiology, and cancer prevention.* Science, 2017. **355**(6331): p. 1330-1334.
3. White, M.C., et al., *Age and Cancer Risk: A Potentially Modifiable Relationship.* American journal of preventive medicine, 2014. **46**(3 0 1): p. S7-15.
4. Catenacci, D.V.T., et al., *Tumor Genome Analysis Includes Germline Genome: Are We Ready for Surprises?* International journal of cancer. Journal international du cancer, 2015. **136**(7): p. 1559-1567.
5. Patel, A.G., J.N. Sarkaria, and S.H. Kaufmann, *Nonhomologous end joining drives poly(ADP-ribose) polymerase (PARP) inhibitor lethality in homologous recombination-deficient cells.* Proc Natl Acad Sci U S A, 2011. **108**(8): p. 3406-11.
6. Du, W., et al., *Hyper-active non-homologous end joining selects for synthetic lethality resistant and pathological Fanconi anemia hematopoietic stem and progenitor cells.* Sci Rep, 2016. **6**: p. 22167.
7. Bouaoun, L., et al., *TP53 Variations in Human Cancers: New Lessons from the IARC TP53 Database and Genomics Data.* Hum Mutat, 2016. **37**(9): p. 865-76.
8. Kaminska, K., et al., *The role of the cell-cell interactions in cancer progression.* J Cell Mol Med, 2015. **19**(2): p. 283-96.
9. Jung, H.Y., L. Fattet, and J. Yang, *Molecular pathways: linking tumor microenvironment to epithelial-mesenchymal transition in metastasis.* Clin Cancer Res, 2015. **21**(5): p. 962-8.
10. Li, H., et al., *The tumor microenvironment: An irreplaceable element of tumor budding and epithelial-mesenchymal transition-mediated cancer metastasis.* Cell Adh Migr, 2016. **10**(4): p. 434-46.
11. Pietila, M., J. Ivaska, and S.A. Mani, *Whom to blame for metastasis, the epithelial-mesenchymal transition or the tumor microenvironment?* Cancer Lett, 2016. **380**(1): p. 359-68.
12. Steen, H.B., *The origin of oncogenic mutations: where is the primary damage?* Carcinogenesis, 2000. **21**(10): p. 1773-6.
13. Capp, J.P., *Tissue disruption increases stochastic gene expression thus producing tumors: Cancer initiation without driver mutation.* Int J Cancer, 2017. **140**(11): p. 2408-2413.
14. Gupta, G.P. and J. Massague, *Cancer metastasis: building a framework.* Cell, 2006. **127**(4): p. 679-95.
15. Li, S., et al., *Model of Tumor Dormancy/Recurrence after Short-Term Chemotherapy.* PLOS ONE, 2014. **9**(5): p. e98021.
16. Zahreddine, H. and K.L. Borden, *Mechanisms and insights into drug resistance in cancer.* Front Pharmacol, 2013. **4**: p. 28.
17. Mezawa, Y. and A. Orimo, *The roles of tumor- and metastasis-promoting carcinoma-associated fibroblasts in human carcinomas.* Cell Tissue Res, 2016. **365**(3): p. 675-89.
18. Jones, S., et al., *Personalized genomic analyses for cancer mutation discovery and interpretation.* Sci Transl Med, 2015. **7**(283): p. 283ra53.
19. Kristina Kjærheim, J.I.M., Hilde Langseth, Tone Eggen og Tom K. Grimsrud, *Cancer in Norway 2015 - Cancer incidence, mortality, survival and prevalence in Norway*. 2016, Oslo: Cancer Registry of Norway: Cancer Registry of Norway.
20. Doubeni, C.A., A.R. Doubeni, and A.E. Myers, *Diagnosis and Management of Ovarian Cancer.* Am Fam Physician, 2016. **93**(11): p. 937-44.
21. Schorge, J.O., C. McCann, and M.G. Del Carmen, *Surgical Debulking of Ovarian Cancer: What Difference Does It Make?* Reviews in Obstetrics and Gynecology, 2010. **3**(3): p. 111-117.

22. Ahmed, N. and K.L. Stenvers, *Getting to know ovarian cancer ascites: opportunities for targeted therapy-based translational research.* Front Oncol, 2013. **3**: p. 256.

23. Rojas, V., et al., *Molecular Characterization of Epithelial Ovarian Cancer: Implications for Diagnosis and Treatment.* Int J Mol Sci, 2016. **17**(12).

24. Meinhold-Heerlein, I., et al., *The new WHO classification of ovarian, fallopian tube, and primary peritoneal cancer and its clinical implications.* Arch Gynecol Obstet, 2016. **293**(4): p. 695-700.

25. Kurman, R.J., *Origin and molecular pathogenesis of ovarian high-grade serous carcinoma.* Ann Oncol, 2013. **24 Suppl 10**: p. x16-21.

26. *Integrated genomic analyses of ovarian carcinoma.* Nature, 2011. **474**(7353): p. 609-615.

27. Garg, K., et al., *p53 overexpression in morphologically ambiguous endometrial carcinomas correlates with adverse clinical outcomes.* Mod Pathol, 2010. **23**(1): p. 80-92.

28. Bowtell, D.D., et al., *Rethinking ovarian cancer II: reducing mortality from high-grade serous ovarian cancer.* Nat Rev Cancer, 2015. **15**(11): p. 668-79.

29. Amate, P., et al., *Ovarian cancer: sites of recurrence.* Int J Gynecol Cancer, 2013. **23**(9): p. 1590-6.

30. Bergamini, A., et al., *Different Patterns of Disease Spread between Advanced-Stage Type I and II Epithelial Ovarian Cancer.* Gynecol Obstet Invest, 2016. **81**(1): p. 10-4.

31. Freyer, G., et al., *Routine Clinical Practice for Patients With Recurrent Ovarian Carcinoma: Results From the TROCADERO Study.* Int J Gynecol Cancer, 2016. **26**(2): p. 240-7.

32. Griffiths, R.W., et al., *Outcomes after multiple lines of chemotherapy for platinum-resistant epithelial cancers of the ovary, peritoneum, and fallopian tube.* Int J Gynecol Cancer, 2011. **21**(1): p. 58-65.

33. Lloyd, K.L., I.A. Cree, and R.S. Savage, *Prediction of resistance to chemotherapy in ovarian cancer: a systematic review.* BMC Cancer, 2015. **15**: p. 117.

34. Yu, K.H., et al., *Predicting Ovarian Cancer Patients' Clinical Response to Platinum-Based Chemotherapy by Their Tumor Proteomic Signatures.* J Proteome Res, 2016. **15**(8): p. 2455-65.

35. Arienti, C., et al., *Peritoneal carcinomatosis from ovarian cancer: chemosensitivity test and tissue markers as predictors of response to chemotherapy.* J Transl Med, 2011. **9**: p. 94.

36. Miyamoto, K., et al., *Disposition kinetics of taxanes in peritoneal dissemination.* Gastroenterol Res Pract, 2012. **2012**: p. 963403.

37. Yan, T.D., et al., *Perioperative intraperitoneal chemotherapy for peritoneal surface malignancy.* J Transl Med, 2006. **4**: p. 17.

38. Van der Speeten, K., O.A. Stuart, and P.H. Sugarbaker, *Pharmacology of perioperative intraperitoneal and intravenous chemotherapy in patients with peritoneal surface malignancy.* Surg Oncol Clin N Am, 2012. **21**(4): p. 577-97.

39. Walker, J.L., *Intraperitoneal chemotherapy requires expertise and should be the standard of care for optimally surgically resected epithelial ovarian cancer patients.* Ann Oncol, 2013. **24 Suppl 10**: p. x41-45.

40. Lotti, M., et al., *Laparoscopic HIPEC: A bridge between open and closed-techniques.* J Minim Access Surg, 2016. **12**(1): p. 86-9.

41. Sugarbaker, P.H., O.A. Stuart, and L. Bijelic, *Intraperitoneal gemcitabine chemotherapy as an adjuvant treatment for patients with resected pancreatic cancer: Phase II and pharmacologic studies.* Translational Gastrointestinal Cancer, 2012. **1**(2): p. 161-168.

42. Yan, T.D., et al., *Cytoreductive surgery and hyperthermic intraperitoneal chemotherapy for malignant peritoneal mesothelioma: multi-institutional experience.* J Clin Oncol, 2009. **27**(36): p. 6237-42.

43. Spiliotis, J., et al., *Mapping the location of peritoneal metastases using the peritoneal cancer index and the correlation with overall survival: a retrospective study.* J BUON, 2015. **20 Suppl 1**: p. S64-70.

44. Hotouras, A., et al., *Heated IntraPEritoneal Chemotherapy (HIPEC) for Patients With Recurrent Ovarian Cancer: A Systematic Literature Review.* Int J Gynecol Cancer, 2016. **26**(4): p. 661-70.

45. Moon, E.J., et al., *NADPH oxidase-mediated reactive oxygen species production activates hypoxia-inducible factor-1 (HIF-1) via the ERK pathway after hyperthermia treatment.* Proc Natl Acad Sci U S A, 2010. **107**(47): p. 20477-82.

46. van den Tempel, N., M.R. Horsman, and R. Kanaar, *Improving efficacy of hyperthermia in oncology by exploiting biological mechanisms.* Int J Hyperthermia, 2016. **32**(4): p. 446-54.

47. Ostberg, J.R., E. Kabingu, and E.A. Repasky, *Thermal regulation of dendritic cell activation and migration from skin explants.* Int J Hyperthermia, 2003. **19**(5): p. 520-33.

48. Mace, T.A., et al., *Effector CD8+ T cell IFN-gamma production and cytotoxicity are enhanced by mild hyperthermia.* Int J Hyperthermia, 2012. **28**(1): p. 9-18.

49. Toraya-Brown, S. and S. Fiering, *Local tumour hyperthermia as immunotherapy for metastatic cancer.* International Journal of Hyperthermia, 2014. **30**(8): p. 531-539.

50. Schaaf, L., et al., *Hyperthermia Synergizes with Chemotherapy by Inhibiting PARP1-Dependent DNA Replication Arrest.* Cancer Res, 2016. **76**(10): p. 2868-75.

51. van Oorschot, B., et al., *Targeting DNA double strand break repair with hyperthermia and DNA-PKcs inhibition to enhance the effect of radiation treatment.* Oncotarget, 2016. **7**(40): p. 65504-65513.

52. Oei, A.L., et al., *Effects of hyperthermia on DNA repair pathways: one treatment to inhibit them all.* Radiation Oncology (London, England), 2015. **10**: p. 165.

53. Slimen, I.B., et al., *Reactive oxygen species, heat stress and oxidative-induced mitochondrial damage. A review.* Int J Hyperthermia, 2014. **30**(7): p. 513-23.

54. Hou, C.H., et al., *Hyperthermia induces apoptosis through endoplasmic reticulum and reactive oxygen species in human osteosarcoma cells.* Int J Mol Sci, 2014. **15**(10): p. 17380-95.

55. Neznanov, N., et al., *Proteotoxic stress targeted therapy (PSTT): induction of protein misfolding enhances the antitumor effect of the proteasome inhibitor bortezomib.* Oncotarget, 2011. **2**(3): p. 209-21.

56. Wang, X., et al., *HSP27, 70 and 90, anti-apoptotic proteins, in clinical cancer therapy (Review).* Int J Oncol, 2014. **45**(1): p. 18-30.

57. Stankiewicz, A.R., et al., *Hsp70 inhibits heat-induced apoptosis upstream of mitochondria by preventing Bax translocation.* J Biol Chem, 2005. **280**(46): p. 38729-39.

58. Multhoff, G., et al., *The role of heat shock protein 70 (Hsp70) in radiation-induced immunomodulation.* Cancer Lett, 2015. **368**(2): p. 179-84.

59. Kimura, A., et al., *Nuclear heat shock protein 110 expression is associated with poor prognosis and chemotherapy resistance in gastric cancer.* Oncotarget, 2016. **7**(14): p. 18415-23.

60. Vargas-Roig, L.M., et al., *Heat shock protein expression and drug resistance in breast cancer patients treated with induction chemotherapy.* Int J Cancer, 1998. **79**(5): p. 468-75.

61. Foster, C.S., et al., *Hsp-27 expression at diagnosis predicts poor clinical outcome in prostate cancer independent of ETS-gene rearrangement.* Br J Cancer, 2009. **101**(7): p. 1137-44.

62. Rappa, F., et al., *Comparative analysis of Hsp10 and Hsp90 expression in healthy mucosa and adenocarcinoma of the large bowel.* Anticancer Res, 2014. **34**(8): p. 4153-9.

63. Sekihara, K., et al., *Pifithrin-mu, an inhibitor of heat-shock protein 70, can increase the antitumor effects of hyperthermia against human prostate cancer cells.* PLoS One, 2013. **8**(11): p. e78772.

64. Pedersen, K.S., et al., *Phase II trial of gemcitabine and tanespimycin (17AAG) in metastatic pancreatic cancer: a Mayo Clinic Phase II Consortium study.* Invest New Drugs, 2015. **33**(4): p. 963-8.

65. Marth, C., et al., *Modulation of ovarian carcinoma OV632 antigen by interferons.* Oncology, 1992. **49**(1): p. 53-7.

66. Bast, R.C., Jr., et al., *Reactivity of a monoclonal antibody with human ovarian carcinoma.* J Clin Invest, 1981. **68**(5): p. 1331-7.

67. Snodgrass, R.G., et al., *Mitomycin C inhibits ribosomal RNA: a novel cytotoxic mechanism for bioreductive drugs.* J Biol Chem, 2010. **285**(25): p. 19068-75.

68. Engebraaten, O., et al., *Systemic immunotoxin treatment inhibits formation of human breast cancer metastasis and tumor growth in nude rats.* Int J Cancer, 2000. **88**(6): p. 970-6.

69. Andersson, Y., O. Engebraaten, and O. Fodstad, *Synergistic anti-cancer effects of immunotoxin and cyclosporin in vitro and in vivo.* Br J Cancer, 2009. **101**(8): p. 1307-15.

70. Froysnes, I.S., et al., *Novel Treatment with Intraperitoneal MOC31PE Immunotoxin in Colorectal Peritoneal Metastasis: Results From the ImmunoPeCa Phase 1 Trial.* Ann Surg Oncol, 2017.

71. Andersson, Y., et al., *Phase I trial of EpCAM-targeting immunotoxin MOC31PE, alone and in combination with cyclosporin.* Br J Cancer, 2015. **113**(11): p. 1548-55.

72. Bellone, S., et al., *Overexpression of epithelial cell adhesion molecule in primary, metastatic, and recurrent/chemotherapy-resistant epithelial ovarian cancer: implications for epithelial cell adhesion molecule-specific immunotherapy.* Int J Gynecol Cancer, 2009. **19**(5): p. 860-6.

73. Flatmark, K., et al., *Immunomagnetic detection of micrometastatic cells in bone marrow of colorectal cancer patients.* Clin Cancer Res, 2002. **8**(2): p. 444-9.

74. Andersson, Y., S. Juell, and O. Fodstad, *Downregulation of the antiapoptotic MCL-1 protein and apoptosis in MA-11 breast cancer cells induced by an anti-epidermal growth factor receptor-Pseudomonas exotoxin a immunotoxin.* Int J Cancer, 2004. **112**(3): p. 475-83.

75. Sugarbaker, P.H., D. Chang, and O.A. Stuart, *Hyperthermic intraoperative thoracoabdominal chemotherapy.* Gastroenterol Res Pract, 2012. **2012**: p. 623417.

76. Ceelen, W.P. and M.F. Flessner, *Intraperitoneal therapy for peritoneal tumors: biophysics and clinical evidence.* Nat Rev Clin Oncol, 2010. **7**(2): p. 108-15.

77. Bauer, K., et al., *High HSP27 and HSP70 expression levels are independent adverse prognostic factors in primary resected colon cancer.* Cell Oncol (Dordr), 2012. **35**(3): p. 197-205.

78. Alvarez Secord, A., et al., *TP53 Status is Associated with Thrombospondin1 Expression In vitro.* Front Oncol, 2013. **3**: p. 269.

79. Havrilesky, L.J., et al., *Loss of Expression of the p16 Tumor Suppressor Gene Is More Frequent in Advanced Ovarian Cancers Lacking p53 Mutations.* Gynecologic Oncology. **83**(3): p. 491-500.

80. Stordal, B., et al., *BRCA1/2 mutation analysis in 41 ovarian cell lines reveals only one functionally deleterious BRCA1 mutation.* Mol Oncol, 2013. **7**(3): p. 567-79.

81. Ó hAinmhire, E., et al., *Mutation or Loss of p53 Differentially Modifies TGFβ Action in Ovarian Cancer.* PLOS ONE, 2014. **9**(2): p. e89553.

82. Domcke, S., et al., *Evaluating cell lines as tumour models by comparison of genomic profiles.* Nature Communications, 2013. **4**: p. 2126.

83. Shaw, T.J., et al., *Characterization of intraperitoneal, orthotopic, and metastatic xenograft models of human ovarian cancer.* Mol Ther, 2004. **10**(6): p. 1032-42.

84. Wiiger, M.T., et al., *The MOC31PE immunotoxin reduces cell migration and induces gene expression and cell death in ovarian cancer cells.* J Ovarian Res, 2014. **7**: p. 23.

85. Mangioni, C., et al., *Randomized trial in advanced ovarian cancer comparing cisplatin and carboplatin.* J Natl Cancer Inst, 1989. **81**(19): p. 1464-71.

86. Boisen, M.M., et al., *Hyperthermic intraperitoneal chemotherapy for epithelial ovarian cancers: is there a role?* Journal of Gastrointestinal Oncology, 2016. **7**(1): p. 10-17.

87. Deraco, M., et al., *Secondary cytoreductive surgery and hyperthermic intraperitoneal chemotherapy for recurrent epithelial ovarian cancer: a multi-institutional study.* BJOG: An International Journal of Obstetrics & Gynaecology, 2012. **119**(7): p. 800-809.

88. Goodman, M.D., et al., *Chemotherapy for intraperitoneal use: a review of hyperthermic intraperitoneal chemotherapy and early post-operative intraperitoneal chemotherapy.* Journal of Gastrointestinal Oncology, 2016. **7**(1): p. 45-57.

89. Zdanovsky, A.G., et al., *Mechanism of action of Pseudomonas exotoxin. Identification of a rate-limiting step.* J Biol Chem, 1993. **268**(29): p. 21791-9.

90. Beeharry, M.K., et al., *A critical analysis of the cytoreductive surgery with hyperthermic intraperitoneal chemotherapy combo in the clinical management of advanced gastric cancer: an effective multimodality approach with scope for improvement.* Transl Gastroenterol Hepatol, 2016. **1**: p. 77.

91. Spiliotis, J., et al., *Cytoreductive surgery and HIPEC in recurrent epithelial ovarian cancer: a prospective randomized phase III study.* Ann Surg Oncol, 2015. **22**(5): p. 1570-5.

92. Bhatt, A. and O. Glehen, *The role of Cytoreductive Surgery and Hyperthermic Intraperitoneal Chemotherapy (HIPEC) in Ovarian Cancer: A Review.* Indian J Surg Oncol, 2016. **7**(2): p. 188-97.

93. Wu, K.-Y., H.-Z. Wang, and S.-J. Hong, *Mechanism of mitomycin-induced apoptosis in cultured corneal endothelial cells.* Molecular Vision, 2008. **14**: p. 1705-1712.

94. Yan, C., et al., *Mitomycin C Induces Apoptosis in Rheumatoid Arthritis Fibroblast-Like Synoviocytes via a Mitochondrial-Mediated Pathway.* Cellular Physiology and Biochemistry, 2015. **35**(3): p. 1125-1136.

95. Kulkarni, R., et al., *Mitochondrial mutant cells are hypersensitive to ionizing radiation, phleomycin and mitomycin C.* Mutat Res, 2009. **663**(1-2): p. 46-51.

96. Dier, U., et al., *Bioenergetic Analysis of Ovarian Cancer Cell Lines: Profiling of Histological Subtypes and Identification of a Mitochondria-Defective Cell Line.* PLOS ONE, 2014. **9**(5): p. e98479.

97. Hettinga, J.V., et al., *Mechanism of hyperthermic potentiation of cisplatin action in cisplatin-sensitive and -resistant tumour cells.* Br J Cancer, 1997. **75**(12): p. 1735-43.

98. Raaphorst, G.P., et al., *A comparison of hyperthermia cisplatin sensitization in human ovarian carcinoma and glioma cell lines sensitive and resistant to cisplatin treatment.* Cancer Chemother Pharmacol, 1996. **37**(6): p. 574-80.

99. Raaphorst, G.P. and D.P. Yang, *The evaluation of thermal cisplatin sensitization in normal and XP human cells using mild hyperthermia at 40 and 41 degrees C.* Anticancer Res, 2005. **25**(4): p. 2649-53.

100. VanderWaal, R.P., et al., *Delaying S-phase progression rescues cells from heat-induced S-phase hypertoxicity.* J Cell Physiol, 2001. **187**(2): p. 236-43.

101. Kusumoto, T., et al., *Sequence dependence of the hyperthermic potentiation of carboplatin-induced cytotoxicity and intracellular platinum accumulation in HeLa cells.* Br J Cancer, 1993. **68**(2): p. 259-63.

102. Bradford, C.R., et al., *P53 mutation correlates with cisplatin sensitivity in head and neck squamous cell carcinoma lines.* Head Neck, 2003. **25**(8): p. 654-61.

103. Tang, J., et al., *Cell adhesion down-regulates the expression of vacuolar protein sorting 4B (VPS4B) and contributes to drug resistance in multiple myeloma cells.* Int J Hematol, 2015. **102**(1): p. 25-34.

104. Lee, J.M., et al., *A three-dimensional microenvironment alters protein expression and chemosensitivity of epithelial ovarian cancer cells in vitro.* Lab Invest, 2013. **93**(5): p. 528-42.

105. Huang, H.L., et al., *Trypsin-induced proteome alteration during cell subculture in mammalian cells.* J Biomed Sci, 2010. **17**: p. 36.

106. Cornford, P.A., et al., *Heat shock protein expression independently predicts clinical outcome in prostate cancer.* Cancer Res, 2000. **60**(24): p. 7099-105.

107. Rybinski, M., et al., *Modelling the efficacy of hyperthermia treatment.* J R Soc Interface, 2013. **10**(88): p. 20130527.

108. Pennisi, R., P. Ascenzi, and A. di Masi, *Hsp90: A New Player in DNA Repair?* Biomolecules, 2015. **5**(4): p. 2589-618.

109. Liu, G., et al., *Differing clinical impact of BRCA1 and BRCA2 mutations in serous ovarian cancer.* Pharmacogenomics, 2012. **13**(13): p. 1523-35.

110. Risch, H.A., et al., *Prevalence and penetrance of germline BRCA1 and BRCA2 mutations in a population series of 649 women with ovarian cancer.* Am J Hum Genet, 2001. **68**(3): p. 700-10.

111. Pal, T., et al., *BRCA1 and BRCA2 mutations account for a large proportion of ovarian carcinoma cases.* Cancer, 2005. **104**(12): p. 2807-16.

112. Zhao, B., M.T. Hemann, and D.A. Lauffenburger, *Intratumor heterogeneity alters most effective drugs in designed combinations.* Proceedings of the National Academy of Sciences, 2014. **111**(29): p. 10773-10778.

113. Yang, Y.-C. and X.-P. Li, *Clinical significance of intratumor heterogeneity for gynecological carcinoma.* Chronic Diseases and Translational Medicine, 2015. **1**(1): p. 14-17.

114. O'Donovan, M., *A critique of methods to measure cytotoxicity in mammalian cell genotoxicity assays.* Mutagenesis, 2012. **27**(6): p. 615-21.

115. Wang, P., S.M. Henning, and D. Heber, *Limitations of MTT and MTS-based assays for measurement of antiproliferative activity of green tea polyphenols.* PLoS One, 2010. **5**(4): p. e10202.

116. Eastman, A., *Improving anticancer drug development begins with cell culture: misinformation perpetrated by the misuse of cytotoxicity assays.* Oncotarget, 2017. **8**(5): p. 8854-8866.

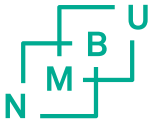

Norges miljø- og biovitenskapelig universitet
Noregs miljø- og biovitskapelege universitet
Norwegian University of Life Sciences

Postboks 5003
NO-1432 Ås
Norway